Two Distinct Sets of Ca 2+ and K + Channels Are Activated at Different Membrane Potentials by the Climbing Fiber Synaptic Potential in Purkinje Neuron Dendrites

Karima Ait Ouares, Luiza Filipis, Alexandra Tzilivaki, Panayiota Poirazi, Marco Canepari

Revised

Two distinct sets of Ca^{2+} and K^+ channels are activated at different membrane potentials by the climbing fibre synaptic potential in Purkinje neuron dendrites

Abbreviated title: *Dendritic ion channels activated by climbing fibre*

Karima Ait Ouares[1,2,*], **Luiza Filipis**[1,2,*], **Alexandra Tzilivaki**[3,4], **Panayiota Poirazi**[3], **Marco Canepari**[1,2,5]

[1]Univ. Grenoble Alpes, CNRS, LIPhy, F-38000 Grenoble, France. [2]Laboratories of Excellence, Ion Channel Science and Therapeutics, France. [3]Institute of Molecular Biology and Biotechnology, Foundation for Research and Technology-Hellas, Heraklion, Crete, Greece. [4]Einstein Center for Neurosciences, Charite Medical School Neuroscience Research Center Berlin, Germany. [5]Institut National de la Santé et Recherche Médicale, France.

*K.A.O. and L.F. contributed equally to this work.

Address of the submitting and corresponding author: Marco Canepari, Laboratoire Interdisciplinaire de Physique (UMR 5588), Bat. E45, 140 avenue de la physique, Domaine univ., 38402 St Martin d'Hères cedex, France. Email: marco.canepari@univ-grenoble-alpes.fr

Number of pages: 22. Number of figures: 10. Number of Tables: 1
Number of words for abstract (250), introduction (642), discussion (1362)

Conflict of interests: *None*

Acknowledgements: This work was supported by the *Agence Nationale de la Recherche* through three grants (ANR-14-CE17-0006 - WaveFrontImag; Labex *Ion Channels Science and Therapeutics:* program number ANR-11-LABX-0015 and National Infrastructure France Life Imaging “Noeud Grenoblois”) and by the *Federation pour la recherché sur le Cerveau* (FRC – Grant *Espoir en tête*, Rotary France). LF was also supported by the EU, through the COST Action CA15124 (NEUBIAS). A.T. and P.P. were supported by the European Research Council Starting Grant dEMORY (GA 311435). AT was supported by Google EMEA Scholarship, by Onassis Foundation MSc Scholarship and by the Einstein Foundation Berlin PhD Fellowship.

Keywords: Cerebellar Purkinje neuron, calcium channels, potassium channels, climbing fibre, neuronal dendrites, NEURON modelling.

Abstract

In cerebellar Purkinje neuron (PN) dendrites, the transient depolarisation associated with a climbing fibre (CF) EPSP activates voltage-gated Ca^{2+} channels (VGCCs), voltage-gated K^+ channels (VGKCs) and Ca^{2+} activated SK and BK K^+ channels. The resulting membrane potential (V_m) and Ca^{2+} transients play a fundamental role in dendritic integration and synaptic plasticity of parallel fibre inputs. Here we report a detailed investigation of the kinetics of dendritic Ca^{2+} and K^+ channels activated by CF-EPSPs, based on optical measurements of V_m and Ca^{2+} transients and on a single-compartment NEURON model reproducing experimental data. We first measured V_m and Ca^{2+} transients associated with CF-EPSPs at different initial V_m and we analysed the changes in the Ca^{2+} transients produced by the block of each individual VGCCs, of A-type VGKCs and of SK and BK channels. Then, we constructed a model that includes six active ion channels to accurately match experimental signals and extract the physiological kinetics of each channel. We found that two different sets of channels are selectively activated. When the dendrite is hyperpolarised, CF-EPSPs mainly activate T-type VGCCs, SK channels and A-type VGKCs that limit the transient V_m below ~0 mV. In contrast, when the dendrite is depolarised, T-type VGCCs and A-type VGKCs are inactivated and CF-EPSPs activate P/Q-type VGCCs, high-voltage activated VGKCs and BK channels, leading to Ca^{2+} spikes. Thus, the potentially activity-dependent regulation of A-type VGKCs, controlling the activation of this second set of channels, is likely to play a crucial role in signal integration and plasticity in PN dendrites.

Significance statement

The climbing fibre synaptic input transiently depolarises the dendrite of cerebellar Purkinje neurons generating a signal that plays a fundamental role in dendritic integration. This signal is mediated by two types of Ca^{2+} channels and four types of K^+ channels. Thus, understanding the kinetics of all of these channels is crucial for understanding PN function. To obtain this information we used an innovative strategy that merges ultrafast optical membrane potential and Ca^{2+} measurements, pharmacological analysis and computational modelling. We found that, according to the initial membrane potential, the climbing fibre depolarising transient activates two distinct sets of channels. Moreover, A-type K^+ channels limit the activation of P/Q-type Ca^{2+} channels and associated K^+ channels, thus preventing the generation of Ca^{2+} spikes.

Introduction

The climbing fibre (CF) synaptic input from the brainstem inferior olive to the cerebellar Purkinje neuron (PN) governs short-term (Brenowitz and Regehr, 2005) and long-term (Safo and Regehr, 2005) synaptic depression of parallel fibre (PF) synaptic inputs in the dendrites. While these important learning mechanisms eventually involve activation of metabotropic glutamate receptors at PF releasing sites and postsynaptic release of endocannabinoids (Marcaggi and Attwell, 2005), the CF signal is carried by a transient depolarisation in the dendrite. The large CF-EPSP is generated in the cell body and in the proximal dendritic segment by glutamate release from hundreds of synaptic terminals (Silver et al., 1998). Then, the depolarisation spreads in the dendritic arborisation (Canepari and Vogt, 2008) where it activates voltage-gated Ca^{2+} channels (VGCCs) and voltage-gated K^+ channels (VGKCs). The transient elevation of intracellular Ca^{2+} activates both SK K^+ channels and BK K^+ channels (Edgerton and Reinhart, 2003). Thus, the ensemble of activated Ca^{2+} and K^+ channels, including VGKCs, shapes the waveform of the dendritic membrane potential (V_m) and of the Ca^{2+} transient, i.e. the two signals that the CF input transmits to the dendritic terminations (Vogt and Canepari, 2010). A detailed characterization of the kinetics of each individual channel involved in the CF signal is therefore crucial for understanding how the CF transmits information to the dendritic arborisation. To tackle this problem, a detailed compartmental model of PNs, including several ion channels, was proposed in the early 90s for predicting the dendritic signals associated with synaptic responses (De Schutter and Bower, 1994). Since then, several computational models incorporating ion channel and morphology variations have been proposed to account for the emerging complex dendritic activity (Anwar et al., 2013; Anwar et al., 2014). Yet, few -if any- of these predictions have been tested experimentally. Importantly, recent advancements in voltage-sensitive dye (VSD) imaging combined with Ca^{2+} imaging with a fast sampling rate, using low-affinity indicators to track the kinetics of VGCCs, allow the direct measurement of V_m and Ca^{2+} signals in the dendrites with a spatial resolution of a few microns (Jaafari et al., 2014; Jaafari et al., 2015; Jaafari and Canepari, 2016).

In this article, we report the first measurements of dendritic V_m and Ca^{2+} transients associated with the CF-EPSP at different initial V_m and the analysis of their correlation. Then, we report a detailed analysis of the changes in the CF-mediated dendritic Ca^{2+} transient produced by the local selective inhibition of various Ca^{2+} or K^+ channels. Based on this rich experimental dataset, obtained from an ensemble of 59 cells, we built a NEURON model of a simplified PN dendritic compartment. The model is based on prior work (Anwar et al., 2012) and incorporates modified channel models to accurately reproduce the V_m and Ca^{2+} transients associated with the CF-EPSP at different initial V_m. The model included P/Q-type high-voltage activated (HVA) VGCCs, T-type low-voltage activated (LVA) VGCCs, A-type LVA-VGKCs and Ca^{2+}-activated K^+ channels (both SK and BK). The consistency of this model was assessed by quantitatively comparing the experimental results of blocking different individual channels, with the elimination of respective channels from the model. The model also included a generic HVA-VGKC (HVAK), an immobile endogenous Ca^{2+} buffer (Canepari and Mammano, 1999), and the two Ca^{2+} binding proteins Calbindin-D28k and Parvalbumin highly expressed in PNs (Schmidt et al., 2003). The

systematic and extensive feedback between experiments and model simulations allowed us unravelling the physiological kinetics of all dendritic Ca^{2+} and K^+ channels activated by the CF-mediated V_m transient, under different initial V_m conditions, providing a realistic model for the ion channels involved. In particular, we found that two distinct sets of channels are activated when the initial resting V_m is either hyperpolarised or depolarised and that the separation between these two sets is governed by the activation of A-type VGKCs that is likely playing a crucial role in regulation and plasticity of PF inputs.

Materials and Methods

SLICE PREPARATION, ELECTROPHYSIOLOGY AND PHARMACOLOGY

Experiments were ethically carried out in accordance with European Directives 2010/63/UE on the care, welfare and treatment of animals. Procedures were reviewed by the ethics committee affiliated to the animal facility of the university (D3842110001). Cerebellar sagittal slices (250 µm thick) were prepared from 21-35 postnatal days old mice (C57Bl6) following established procedures (Vogt et al., 2011a; Vogt et al., 2011b; Ait Ouares et al., 2016) with a Leica VT1200 (Leica, Wetzlar, Germany) and incubated at 37°C for 45 minutes before use. The extracellular solution contained (in mM): 125 NaCl, 26 $NaHCO_3$, 1 $MgSO_4$, 3 KCl, 1 NaH_2PO_4, 2 $CaCl_2$ and 20 glucose, bubbled with 95% O_2 and 5% CO_2. The intracellular solution contained (in mM): 125 $KMeSO_4$, 5 KCl, 8 $MgSO_4$, 5 Na_2-ATP, 0.3 Tris-GTP, 12 Tris-Phosphocreatine, 20 HEPES, adjusted to pH 7.35 with KOH. In combined V_m and Ca^{2+} imaging experiments, PNs were loaded with the voltage-sensitive dye (VSD) JPW1114 and with the Ca^{2+} indicator FuraFF (at 1 mM) using a previously described procedure (Vogt et al., 2011a). In experiments of Ca^{2+} imaging only, Oregon Green BAPTA-5N (OG5N) was added to the internal solution at 2 mM concentration. Patch-clamp recordings were made at 32-34°C using a Multiclamp amplifier 700A (Molecular Devices, Sunnyvale, CA) and signals were acquired at 20 kHz using the A/D board of the CCD camera. The measured V_m was corrected for junction potential (-11 mV) as previously estimated (Canepari et al., 2010). CF -EPSPs were elicited by current pulses, of 5-20 µA amplitude and 100 µs duration delivered by a pipette. Local block of the various channels was achieved by gentle pressure application of the extracellular solution containing the specific blocker at selected effective concentration, using a pipette of ~2 µm diameter. Full names of chemicals used to block L-type, N-type or T-type VGCCs were Isradipine: 4-(2,1,3-Benzoxadiazol-4-yl)-1,4-dihydro-2,6-dimethyl-3,5-pyridinecarboxylic acid methyl 1-methylethyl ester; PD173212: *N*-[[4-(1,1-Dimethylethyl)phenyl]methyl-*N*-methyl-L-leucyl-*N*-(1,1-dimethylethyl)-*O*-phenylmethyl)-L-tyrosinamide; ML218: 3,5-dichloro-*N*-[[(1α,5α,6-exo,6α)-3-(3,3-dimethylbutyl)-3-azabicyclo[3.1.0]hex-6-yl]methyl]-benzamide-hydrochloride; NNC550396: (1*S*,2*S*)-2-[2-[[3-(1*H*-Benzimidazol-2-yl)propyl]methylamino]ethyl]-6-fluoro-1,2,3,4-tetrahydro-1-(1-methylethyl)-2-naphthalenyl-cyclopropanecarboxylate-dihydrochloride. The VSD and the Ca^{2+} indicators were from Invitrogen (Carlsbad, CA). ω-Agatoxin IVA, AmmTx3, iberiotoxin and apamin were purchased from Smartox Biotechnology (St Martin d'Hères, France). All other chemicals were purchased from Tocris (Bristol, UK), from Hello Bio (Bristol, UK) or from Sigma-Aldrich (St. Louis, MO).

OPTICAL SIGNALS RECORDING AND CALIBRATION

Sequential V_m and Ca^{2+} optical measurements (Canepari et al., 2008; Canepari and Ogden, 2008) were achieved by alternating excitation of FuraFF at 385 nm with an OptoLED (CAIRN Research Ltd., Faversham, UK) and of the VSD at 532 nm using a 300 mW solid state laser (model MLL532, CNI, Changchun, China). In experiments with Ca^{2+} imaging only, OG5N was excited at 470 nm with the OptoLED. Ca^{2+} fluorescence (either from FuraFF or from OG5N) and V_m fluorescence were recorded at 525 ± 25 nm and at >610 nm respectively using a NeuroCCD-SMQ camera (RedShirtimaging, Decatur, GA). Images, de-magnified by ~0.2X to visualise an area of ~150 µm diameter, were acquired at 5 kHz with a resolution of 26 X 26 pixels. Electrical and optical signals associated with the CF-EPSP were recorded for 20 ms (100 frames) with the CF stimulation occurring 2 ms after the beginning of trials. 3-4 trials, with 20 s between two consecutive trials, were obtained to assess the consistency of the signals. Fluorescence from these trials was averaged and corrected for bleaching using a filtered trial without signal. V_m and Ca^{2+} signals were initially expressed as fractional changes of fluorescence ($\Delta F/F_0$). To match experimental Ca^{2+} signals with NEURON simulations, $\Delta F/F_0$ was converted into Ca^{2+}-bound-to-dye concentration ($[Ca^{2+}Dye]$) as previously described (Ait Ouares et al., 2016). Briefly, $[Ca^{2+}Dye] = [Dye]_{TOT} \cdot \Delta F/F_0/\sigma$, where $[Dye]_{TOT}$ is the total dye concentration and σ is the empirical *dynamic range* defined as the $\Delta F/F_0$ for saturating Ca^{2+} (Ait Ouares et al., 2016). Measurements of σ were obtained by saturating the indicators in the cytosol with a 30 s step of – 500 mV (in voltage clamp) that makes the somatic membrane permeable to Ca^{2+}. The value of σ obtained in this way for FuraFF was -0.9. VSD $\Delta F/F_0$ was calibrated into a V_m transient using an established procedure (Canepari and Vogt, 2008). Assuming that somatic hyperpolarisations from the resting V_m spread without attenuation through PN dendrites (Roth and Häusser, 2001), a prolonged hyperpolarising step of 1 s was used in each experiment to convert the VSD $\Delta F/F_0$ signal into mV, as shown in the example of Fig. 1A. Since in this study signals associated with the CF-EPSP were evoked at different initial V_m, depolarising steps of 1 s were also used to estimate the dendritic V_m produced by somatic depolarisation. In detail, as shown in the example of Fig.1A, the two largest depolarisation steps lead to the same dendritic V_m although corresponding to two different somatic V_m. This indicates that the dendrite reaches a maximal steady V_m regardless of the current injected into the soma above certain intensity. In our experiments, V_m recordings at depolarised states were performed by injecting currents above this intensity, in this way driving the initial dendritic V_m to the maximal value that was obtained by the calibration protocol.

EXPERIMENTAL DESIGN AND STATISTICAL ANALYSIS

The effects of changing the initial V_m on the V_m and Ca^{2+} transients, or of blocking a Ca^{2+} or a K^+ channel on the Ca^{2+} transients, were established by performing the paired Student's t-test on the signal under the two different conditions. A change in the signal was considered significant when $p < 0.005$. In all figures and tables, a significant change was indicated with "*". The regions of interest used for the

statistical analysis of pharmacological tests were those adjacent to the pipette delivering the channel blocker.

PROCEDURE OF MATCHING EXPERIMENTAL TRANSIENTS WITH A NEURON MODEL

To deduce the kinetics of each channel involved in the dendritic electrical signal associated with the CF-EPSP, we developed an original approach based on matching optical data with a simplified model, implemented in NEURON (Hines and Carnevale, 1997) as depicted in Fig. 1B. To build the model, we started from a published model designed to predict activation of Ca^{2+} activated K^+ channels in PN dendrites (Anwar et al., 2012), available in the ModelDB database at (https://senselab.med.yale.edu/ModelDB/ShowModel.cshtml?model=138382&file=/AnwarEtAl2010/cdp5.mod#tabs-1). From this model, consisting of a cylinder of 4 µm diameter and 20 µm length with standard passive membrane properties, several parameters and mechanisms were initially replaced with those from two earlier models (De Schutter and Bower, 1994; Solinas et al. 2008) also available in ModelDB database at (https://senselab.med.yale.edu/ModelDB/ShowModel.cshtml?model=7176#tabs-1) and at (https://senselab.med.yale.edu/ModelDB/ShowModel.cshtml?model=112685&file=/Golgi_cell/Golgi_SK2.mod#tabs-2). From this starting point, the kinetics of ion channels were changed in order to obtain traces from simulations that matched experimental V_m and Ca^{2+} optical measurements from ~17X17 μm^2 square regions at three different initial V_m: hyperpolarised (~-80 mV), intermediate (~-65 mV) and depolarised (~-50 mV). The specific modifications implemented for each channel are described in detail in the paragraph below. After obtaining a satisfactory set of models for each channel in one cell, the same channel models were used to match our experimental data in three more cells, only by tuning the channel densities and the current input associated with the CF-EPSP.

ION CHANNEL MATHEMATICAL FUNCTIONS MATCHING EXPERIMENTAL DATA

The channel functions that matched experimental V_m and Ca^{2+} transients are reported below and are available in ModelDB at http://senselab.med.yale.edu/ModelDB/showModel.cshtml?model=244679. In detail, I is the current density (expressed in mA/cm^2), $\prod$ is channel permeability to Ca^{2+} (expressed in cm/s), m_∞, t_m, m_{exp} and h_∞, t_h are the voltage-dependent activation and inactivation parameters respectively, z_∞ ,z_{exp} and t_z are the Ca^{2+}-dependent activation parameters, and GHK is the Goldman-Hodgkin-Katz factor (expressing the current per unit permeability, Anwar et al., 2012). Voltage (V) and time are expressed in mV and ms respectively.

- *P/Q-type VGCC*. Starting from the formulation for P/Q-type VGCCs in Anwar et al., 2012, we multiplied the activation curve by a sigmoid function to account for the fact that we did not observe P/Q channel activation below -50 mV. We also reduced the activation time by 40% to reproduce the observed Ca^{2+} spiking rate at depolarised states.

$$\mathrm{I} = \Pi \cdot \mathrm{m}^3 \cdot \mathrm{GHK}$$

$$\mathrm{m}_\infty = \frac{1}{1 + e^{-(V+29.458)/8.439}} \cdot \frac{1}{1 + e^{-0.1 \cdot (V+50)}}$$

$$t_m = \begin{cases} 0.6 \cdot \left(0.2702 + 1.1622 \cdot e^{-\frac{(V+26.798)^2}{164.19}}\right) & \text{if } V \leq -40\text{mV} \\ 0.6 \cdot 0.6923 \cdot e^{V/1089.372} & \text{otherwise} \end{cases}$$

- *T-type VGCC*. Starting from the formulation for T-type VGCCs in Anwar et al., 2012, we multiplied the activation curve by a sigmoid function to account for the observed activation at hyperpolarised and intermediate states. The activation time was decreased by 70% while the inactivation time was doubled to fit the rise and decay of the experimental V_m trace at the hyperpolarised state.

$$I = \Pi \cdot m^2 \cdot h \cdot GHK$$

$$m_\infty = \frac{1}{1 + e^{-(V+51)/6}} * corr$$

$$corr = \begin{cases} \frac{1}{1 + e^{-0.3 \cdot (V+53)}} & \text{at hyperpolarised states} \\ \frac{1}{1 + e^{-0.3 \cdot (V+45)}} & \text{at intermediate states} \end{cases}$$

$$h_\infty = \frac{1}{1 + e^{-(\frac{V+72}{7})}}$$

$$t_m = \begin{cases} 1 & \text{if } V \leq -90\text{mV} \\ \frac{0.2}{e^{(V+40)/9} + e^{-(V+108)/18}} + 0.3 & \text{otherwise} \end{cases}$$

$$t_h = 32 + \frac{2}{e^{(V+32)/7}}$$

- *SK Ca^{2+}-activated K^+ channel*. We used the model in Solinas et al., 2008 with 95% of the SK channels coupled to T-type VGCCs to account for effect of blocking these channels observed exclusively at hyperpolarised states.
- *BK Ca^{2+}-activated K^+ channel*. Starting from the formulation in De Schutter and Bower, 1994, we reduced the Ca^{2+} dependent activation time to half to account for the larger slow repolarisation at depolarised states.

$$I = \Sigma \cdot m \cdot z^2 \cdot (V + 85)$$

$$m_\infty = \frac{8.5}{7.5 + a_m}$$

$$z_\infty = \frac{1}{1 + a_z}$$

$$a_m = \frac{0.11}{e^{(V-55)/14.9}}$$

$$a_z = \frac{0.4}{[Ca^{2+}]}$$

$$m_{exp} = 1 - e^{-0.002*(7.5+a_m)}$$

$$z_{exp} = 1 - e^{-0.0005}$$

- *A-type VGKC*. Starting from the formulation of A-type VGKCs channels in De Schutter and Bower, 1994, the kinetic parameters were modified in line with modifications of T-type VGCCs to account for behaviours at hyperpolarised states. The density was corrected at intermediate states to account for partial inactivation.

$$I = \Sigma \cdot h \cdot m^4 \cdot (V + 85)$$

$$m_\infty = \frac{a_m}{a_m + b_m} \cdot \frac{1}{1 + e^{-0.2 \cdot (V+50)}}$$

$$h_\infty = \frac{a_h}{a_h + b_h}$$

$$a_m = \frac{1.4}{1 + e^{-(V+50)/12}}$$

$$a_h = \frac{0.0175}{1 + e^{(V+85)/8}}$$

$$b_m = \frac{0.49}{1 + e^{(V+30)/4}}$$

$$b_h = \frac{1.3}{1 + e^{-(V+13)/10}}$$

$$t_m = \frac{1}{a_m + b_m}$$

$$t_h = \frac{1}{a_h + b_h}$$

- *HVA-VGKC (HVAK)*. Starting from the formulation of the “delayed rectifier channel” given in De Schutter and Bower, 1994, The HVAK kinetic parameters were modified to account for the behaviours at depolarised states. Specifically, the activation curve was multiplied by a sigmoid function to track the occurrence of the first Ca^{2+} spike. Then the activation time was decreased by ~95% to reproduce the number and shape of the observed Ca^{2+} spikes. Notably, this is the only channel for which the experimental pharmacological block was not available.

$$I = \Sigma \cdot h \cdot m^2 \cdot (V + 85)$$

$$m_\infty = \frac{a_m}{a_m + b_m} \cdot \frac{1}{1 + e^{-0.4 \cdot (V+35)}}$$

$$h_\infty = \frac{1}{1 + e^{(V+25)/4}}$$

$$a_m = \frac{-0.0047 \cdot (V - 8)}{-0.9999 + e^{-(V-8)/12}}$$

$$b_m = e^{-(V+127)/30}$$

$$t_m = \frac{0.055}{\frac{-0.0047 * (V + 12)}{-0.9999 + e^{-(V+12)/12}} + e^{-\frac{V+147}{30}}}$$

$$t_h = \begin{cases} 1200 \text{ if } V < -25 \\ 10 \text{ otherwise} \end{cases}$$

MODEL OF THE CF-ASSOCIATED CURRENT

The model of the current associated with a CF-EPSP, designed to mimic the shape of the current reported by Llano et al., 1991, was expressed by the equation:

$$I_{CF} = I_{HOLD} + I_{STANDING} \cdot \left(1 - e^{-(t-DELAY)/RISE}\right) \cdot e^{-(t-DELAY)/DURATION}$$

The parameters in this equation were tuned to obtain the match of experimental V_m and Ca^{2+} transients within the following ranges. I_{HOLD} (holding current before CF-EPSP occurrence): between -0.03 and 0.04 mA/cm^2. $I_{STANDING}$: between -0.4 and -0.1 mA/cm^2. DELAY: between 2 and 2.4 ms. RISE: between 0.4 and 1.8 ms. DURATION: between 2.5 and 6.

OTHER FIXED MECHANISMS AND PARAMETERS OF THE NEURON MODEL

The following standard mechanism parameters in Fig. 1B, were used in the simulations.

- Immobile buffer (concentration and Ca^{2+} reaction kinetic parameters, from Ait Ouares et al. 2016): concentration = 1 mM; K_{ON} = 570 μM^{-1}s^{-1}; K_{OFF} = 5.7·10^3 s^{-1}.
- Parvalbumin (concentration and Ca^{2+} reaction kinetic parameters for Ca^{2+} and for Mg^{2+}, corrected from empirical values reported in Lee et al., 2000 to take into account the difference in temperature and radial diffusion): binding sites concentration (two per molecule) = 150 μM; K_{ON}^{Ca2+} = 535 μM^{-1}s^{-1}; K_{OFF}^{Ca2+} = 0.95 s^{-1}; K_{ON}^{Mg2+} = 4 μM^{-1}s^{-1}; K_{OFF}^{Mg2+} = 25 s^{-1}.
- Calbindin D28-k (concentration and Ca^{2+} reaction kinetic parameters, corrected from empirical values reported in Nägerl et al., 2000 to take into account the difference in temperature and radial diffusion): fast binding sites concentration (two per molecule) = 1.2 mM; K_{ON} = 217.5 μM^{-1}s^{-1}; K_{OFF} = 35.8 s^{-1}; slow binding sites concentration (two per molecule) = 1.2 mM; K_{ON} = 27.5 μM^{-1}s^{-1}; K_{OFF} = 2.6 s^{-1}.
- Ca^{2+} indicator (Ca^{2+} reaction kinetic parameters): K_{ON} = 570 μM^{-1}s^{-1}; concentration FuraFF = 1 mM; K_{OFF}(FuraFF) = 5.7·10^3 s^{-1}; concentration OG5N = 2 mM; K_{OFF}(OG5N) = 19.95·10^3 s^{-1} ;
- Ca^{2+} extrusion equation was adopted from Destexhe et al., 1993, with kinetic parameters and density used in Anwar et al., 2012: K_{ON} = 3·10^{-3} μM^{-1} s^{-1}; K_{OFF} = 1.75·10^{-2} s^{-1}; K_{EXT} = 7.255·10^{-5} μM^{-1} s^{-1}; density = 10^{-9} mol cm^{-2};
- LEAK current: 0.002 mA/(mV·cm^2)· (V_{init}-V_{rest}), where V_{init} is the initial V_m (in mV) and V_{rest} is the resting V_m (-65 mV).

Results

Dendritic depolarisation and Ca^{2+} transients associated with the CF-EPSP

In the first series of experiments (N = 12 cells), we investigated the dendritic depolarisation and the Ca^{2+} transients associated with the CF-EPSP by combining V_m and Ca^{2+} imaging as described in the Materials and Methods. Within a recording field of ~150X150 μm^2 (26X26 pixels), we systematically averaged fluorescence over 1-3 dendritic regions of ~17X17 μm^2 (3X3 pixels) with sufficient signal-to-noise ratio in order to reliably measure $\Delta F/F_0$ signals with both indicators, at 5 kHz. In each cell and dendritic region, the V_m was determined from voltage sensitive dye $\Delta F/F_0$ signals using the protocol described in the Materials and Methods and illustrated in Fig. 1A. In the cell reported in Fig. 2A, the initial somatic V_m was set by current injection and a CF-EPSP was evoked at a state of hyperpolarisation (*hyp*, blue trace) around -80 mV, at an intermediate V_m (*int*, green trace) close to the resting V_m, and at a state of depolarisation (*dep*, red trace). These three conditions corresponded, in this particular cell, to initial dendritic V_m of -83 mV, -64 mV and -54 mV respectively. In the two analysed regions (*R1* and *R2*), the dendritic V_m transient associated with the CF-EPSP had a first peak occurring within 3 ms after the stimulation that ranged from -17 mV at the *hyp* state to +10 mV at the *int* state (Fig. 2B). A second sharp peak was observed at the *dep* state. Correlated with these V_m transients, the Ca^{2+} transient increased from the *hyp* state to the *int* state and exhibited two sharp peaks at the *dep* state that can be defined as *spikes* since they are characterised by a rapid rise and fall. This behaviour was consistently observed in every cell investigated. The V_m and Ca^{2+} transients in *R1* are shown again in Fig. 2C to illustrate the quantitative analysis that was performed. For both dendritic V_m and Ca^{2+} transients, we measured the maximum (max) during the first 4 ms after the CF stimulation (1^{st} max) and between 4 and 14 ms after the CF stimulation (2^{nd} max). The values for *R1* are reported in Fig. 2C and the statistics (mean ± SD) for 19 regions in the 12 cells analysed are reported in Fig. 2D. At *hyp* states (with initial V_m between -87 mV and -74 mV), the 1^{st} and 2^{nd} V_m maxima were -13 ± 8 mV and -38 ± 7 mV respectively, while the Ca^{2+} transient ($-\Delta F/F_0$) max were 1.83 ± 0.55 % and 3.14 ± 0.85 % respectively. At *int* states (with initial V_m between -68 mV and -61 mV), the 1^{st} and 2^{nd} V_m maxima were 6 ± 7 mV and -21 ± 11 mV respectively, while the Ca^{2+} transient max were 3.65 ± 1.27 % and 3.65 ± 1.05 % respectively. Finally, at *dep* states (with initial V_m between -54 mV and -46 mV), the 1^{st} and 2^{nd} V_m maxima were 9 ± 6 mV and -1 ± 9 mV respectively, while the Ca^{2+} transients maxima were 5.36 ± 1.17 % and 6.59 ± 1.42 % respectively. The 1^{st} max of both V_m and Ca^{2+} transients significantly increased from the *hyp* state to the *int* state ($p < 0.005$, paired t-test), while the 2^{st} max of both the V_m and Ca^{2+} transients significantly increased from the *int* state to the *dep* state. These results demonstrate that CF-EPSP associated dendritic depolarisation and Ca^{2+} influx increase with the initial V_m. Furthermore, dendritic spikes (typically two in the 18 ms after the stimulation) and correlated Ca^{2+} transients occur when the dendrite is depolarised. The dendritic depolarisation is produced by the passive spread of the CF-EPSP from the soma and proximal dendrite and activates voltage-gate Ca^{2+} channels (VGCCs) and voltage-gate K^+ channels (VGKCs). Ca^{2+}-

activated K^+ channels contribute to the repolarisation. To resolve the channels underlying the behaviours observed in the experiments reported above, we analysed pharmacologically in detail the Ca^{2+} transient associated with the CF-EPSP.

Dendritic Ca^{2+} channels activated by the CF-EPSP

In PNs, the dendritic Ca^{2+} transients associated with the CF-EPSP transient depolarisation are mediated by VGCCs, in particular P/Q-type HVA-VGCCs (Usowitz et al., 1992) and T-type LVA-VGCCs (Isope et al., 2012). Thus, we investigated the changes in the Ca^{2+} transients from OG5N fluorescence produced by the selective block of one or more VGCCs. In the representative example of Fig. 3A, the CF-EPSP was evoked at *hyp* (blue traces), *int* (green traces) and *dep* (red traces) states and the associated OG5N- $\Delta F/F_0$ signal was recorded in the control condition and after local application of the P/Q-type VGCC blocker ω-agatoxin-IVA (AgaIVA, 1 µM). Importantly, to assess the postsynaptic effect while excluding any possible presynaptic effect, the changes in the Ca^{2+} transient were analysed and compared in the region next to the application pipette (*R1*) and in another region at more than 50 µm from the application pipette (*R2*). In *R1* only, AgaIVA reduced the Ca^{2+} transient during the first few milliseconds after the CF-EPSP at the *hyp* and *int* states, and blocked the Ca^{2+} transient at the *dep* state. In the representative example of Fig. 3B, the same protocol was used to assess the effects of local block of T-type VGCCs, using the inhibitors ML218 (ML, 5 µM) and NNC550396 (NNC, 30 µM). In this case, the blockers inhibited the late component of the Ca^{2+} transient at the *hyp* and *int* states, but had no effect on the Ca^{2+} transient at the *dep* state. Finally, in the representative example of Fig. 3C, local block of P/Q-type and T-type VGCCs together inhibited Ca^{2+} transient in all states. To rule out any additional component from other VGCC types, in the three representative examples of Fig. 3D, we also tested the blockers Isradipine (20 µM, L-type), PD173212 (5 µM, N-type) and SNX482 (1 µM, R-type). The Ca^{2+} transient remained unaffected under all states and cases tested. The results reported in Fig. 3 were consistently observed in all cells tested with each VGCC blocker. To quantify these results, we measured again the 1st max (during the first 4 ms after the stimulation) and the 2nd max (between 4 ms and 14 ms after the stimulation), and calculated the percentage of the two maxima in the presence of the VGCC blocker, with respect to the control condition, as illustrated in the examples of Fig. 4. We tested the block of P/Q-type VGCCs (AgaIVA), of T-type VGCC (ML + NNC) or of P/Q-type and T-type VGCCs together (AgaIVA + ML + NNC) in N = 6 cells for each case. The block of P/Q channels significantly reduced the 1st max of the Ca^{2+} transient at all initial V_m states ($p < 0.005$, paired t-test), while the 2nd max was reduced only in the *int* and *dep* states. In contrast, the block of T channels significantly reduced the 1st and 2nd maxima of the Ca^{2+} transient at *hyp* states and the 2nd max only and *int* states, while neither max was changed at *dep* states. The block of P/Q and T channels together significantly reduced both maxima at all initial states. Finally, we tested the block of L-type VGCCs (Isr), of N-type VGCC (PD) or of R-type VGCCs (SNX) in N = 4 cells for each case. No changes in the two maxima were observed in any of the initial states. In summary, these results show the distinct kinetics of two components of Ca^{2+} influx, associated with the CF-EPSP and mediated by P/Q-type and T-type VGCCs respectively. At *hyp*

states, where the depolarisation transient is typically below -10 mV (see Fig. 2), P/Q-type VGCCs are weakly activated, but activation of these channels increases when the initial V_m becomes more positive and the transient depolarisation larger. In contrast, T-type VGCCs are strongly activated at *hyp* states, but these channels inactivate as the initial V_m increases.

Dendritic K^+ channels activated by the CF-EPSP

Activation of dendritic P/Q-type VGCCs at *int* and *dep* states is correlated with larger depolarisation transients associated with CF-EPSPs, possibly due to steady inactivation of A-type VGKCs that are expressed in PN dendrites (Otsu et al., 2014). To test this hypothesis, we investigated the change in the OG5N Ca^{2+} transient produced by local application of the A-type VGKC inhibitor AmmTx3 (Zoukimian et al., *in press*). As shown in the representative example of Fig. 5A, the block of A-type channels strongly enhanced the Ca^{2+} transient associated with the CF-EPSP both at the *hyp* and *int* states, but did not produce any effect at the *dep* state. In contrast to the experiments with VGCC blockers, the effect of AmmTx3 was not observed exclusively in the area adjacent to the pipette delivering the toxin (data not shown). In N = 6 cells tested, AmmTx3 significantly enhanced the 1^{st} and 2^{nd} maxima of the Ca^{2+} transient at *hyp* and *int* states, also at sites located at >50 µm from the pipette delivering the toxin, while it did not modify the Ca^{2+} transient at *dep* states indicating that A-type VGKCs are fully inactivated at initial V_m > -55 mV (Fig. 5B). In contrast A-type VGKCs are activated at more negative initial V_m and this result suggests that their activation limits the activation of P/Q-type VGCCs.

Since Ca^{2+} transients activate Ca^{2+}-activated K^+ channels, we finally investigated the change in the OG5N Ca^{2+} transient produced by local application of the BK channel inhibitor iberiotoxin (1 µM, Fig. 6A) and of the SK channel inhibitor apamin (1µM, Fig. 6B). Neither iberiotoxin nor apamin produced any change in the 1^{st} and 2^{nd} maxima of the Ca^{2+} transient at *hyp*, *int* and *dep* states, a result observed in N = 5 cells tested with iberiotoxin and N = 6 cells tested with apamin (Fig. 6C). Nevertheless, in 5/5 cells where the block of BK channels was tested, the number of Ca^{2+} spikes increased from 2 to 3 at *dep* states. In addition, in 4/6 cells where the block of SK channels was tested, a slight but observable decrease in the decay of the OG5N $\Delta F/F_0$ signal was noticed (Fig.6D). These two results indicate that both channels are activated by the CF-EPSP at different initial V_m states.

Analysis of dendritic ion currents associated with the CF-EPSP by NEURON modelling

To extrapolate individual dendritic ion currents underlying V_m transients and Ca^{2+} signals associated with CF-EPSPs at different V_m initial states, we selected 4 dendritic sites from 4 different PNs within those analysed in Fig. 2. The criterion for the selection was that the somatic resting V_m and CF-EPSP at different initial V_m were stable for the entire duration of the recordings, in order to assume the same conditions for the V_m and Ca^{2+} recordings. In these 4 compartments, we matched the experimental V_m and Ca^{2+} transients with traces obtained by computer simulations of the NEURON model illustrated in Fig. 1B, as described in the Materials and Methods. In particular, we established a unique kinetic model for each of the six types of channels, in order to consistently reproduce the behaviours observed in all 4

cells. The model that matches V_m and Ca^{2+} transients is available in the ModelDB database at http://senselab.med.yale.edu/ModelDB/showModel.cshtml?model=244679. While the channel kinetics were the same in all simulations, the density of P/Q-type and T-type VGCCs, of A-type and HVAK VGKCs, and of BK and SK Ca^{2+} activated K^+ channels was adjusted in order to match experimental data in each cell, as shown in Fig. 7. To validate the consistency of the four variants of the model, we run computer simulations by modelling the replacement of 1 mM Fura-FF with 2 mM OG5N and analysed Ca^{2+} $\Delta F/F_0$ modifications produced by the elimination of 90% of each channel, in this way mimicking the experiments in which individual channels were pharmacologically blocked. As an example, the results for the model variant of cell 1 in Fig. 7 are reported in Fig. 8, showing that 90% reduction in the density of each channel qualitatively reproduced the experimental behaviour observed after toxin or drug inhibition. In order to compare experiments and simulations, we calculated the percentage of the 1st max and the 2nd max of the Ca^{2+} transient after elimination of 90% of each channel. The comparisons, reported in Table 1, indicate that the observed effects on Ca^{2+} signals in the experiments are all in line with the predictions from the simulations. In addition, in all 4 variants of the model, the 90% reduction of BK channels reproduced the appearance of a third Ca^{2+} spike that was also observed in experiments. In summary, matching experimental data with NEURON simulations generated a simplified yet biological plausible dendritic model that successfully reproduces the complexity of experimental signals.

We then used the model variant of cell 1 of Fig. 7 to extrapolate the kinetics of each channel contributing to the CF-mediated signal under different conditions (Fig. 9). At *hyp* state (blue traces), the depolarisation transient carried by the CF-EPSP activates a robust Ca^{2+} current, mediated by T-type channels, and a K^+ current, mediated by A-type channels. A very small K^+ current mediated by SK channels is elicited by the transient Ca^{2+} elevation. P/Q-type VGCCs and HVAK VGKSs are poorly activated in this state. As the initial V_m becomes more positive (*int* state, green traces), part of T-type and A-type channels become inactivated, reducing the associated currents and allowing more P/Q and HVAK channels to activate. Finally, at *dep* state (red traces), T-type and A-type channels are fully inactivated and the depolarisation transient carried by the CF-EPSP activates a Ca^{2+} current, mediated by P/Q-type Ca^{2+} channels, and a K^+ current, mediated by HVAK channels, which are responsible for multiple Ca^{2+} spikes. The number of spikes is limited by the K^+ current mediated by BK channels. The strong activation of P/Q-type VGCCs and HVAK VGKCs is prevented at *hyp* states by the K^+ current mediated by A-type VGKCs. Hence, when A-type channels are reduced by 90% (purple traces), activation of P/Q-type VGCCs is strongly enhanced, substantially increasing the dendritic Ca^{2+} transient. In summary, by extrapolating the kinetics of individual Ca^{2+} and K^+ channels, we resolved their functional interaction establishing a specific role of A-type VGKCs in controlling activation of P/Q-type channels, HVAK channels and BK channels.

Discussion

In this article, we report an original study of the dendritic V_m and Ca^{2+} transients associated with the CF-EPSP at different initial V_m. We explored experimentally, using combined V_m and Ca^{2+} imaging, the activation of five Ca^{2+} or K^+ channels and we propose a simplified single compartment model that produces simulations of the V_m and Ca^{2+} transients that accurately match experimental data. Interestingly, we used 4 stable cells for this analysis and the matching models were obtained using the same kinetic models of the six channels with relatively small variations of conductance densities. Using this strategy, which combines fast imaging techniques, pharmacological analysis and biophysical modelling, we unravelled the precise kinetics of dendritic Ca^{2+} and K^+ channel activation in PNs during CF-EPSPs under different V_m conditions. In particular, we established a clear role for the A-type VGKC in limiting the membrane depolarisation and the activation of P/Q-type VGCCs.

Two distinct sets of channels activated by the CF-EPSP

We found that two different sets of channels are selectively activated at different initial V_m. When the dendrite is hyperpolarised (V_m ~ -80 mV), the transient depolarisation produced by the CF-EPSP invading the dendritic branch activates T-type VGCCs (Isope et al., 2012) that enhance the distal dendritic V_m depolarisation produced by the spread of the EPSP. The dendritic V_m is however capped below ~10 mV by the K^+ current via A-type VGKCs, limiting the opening of HVA Ca^{2+} and K^+ channels. Under this condition, Ca^{2+} influx activates SK channels (Hosy et al., 2011) that regulate V_m repolarisation and that appear selectively linked to T-type VGCCs, presumably by molecular coupling (Stocker, 2004). When in contrast the dendrite is depolarised (V_m ~ -50 mV), T-type VGCCs and A-type VGKCs are inactivated and the CF-EPSP can drive the dendrite to more positive V_m values that activate first P/Q-type VGCCs (Usowicz et al., 1992) and then HVAKs leading to Ca^{2+} spikes (see the channels model available at http://senselab.med.yale.edu/ModelDB/showModel.cshtml?model=244679). In this case, Ca^{2+} influx activates BK channels (Rancz and Häusser, 2006) that fasten V_m repolarisation limiting the number of Ca^{2+} spikes. HVAKs include Kv3.3 that is highly expressed in PNs (Goldman-Wohl et al., 1994), regulating dendritic Ca^{2+} spikes (Zagha et al., 2010; Veys et al., 2013). However, the lack of a selective channel blocker for this VGKC didn't permit the experimental assessment of the kinetics of this channel and we cannot exclude a contribution of other VGKCs with similar biophysical properties. The role of BK channels is to dampen the generation of Ca^{2+} spikes, which are typically only two when these channels are active. Finally, significant activation of both sets of channels occurs only at intermediate initial V_m (~ -65 mV). In summary, The CF-evoked dendritic Ca^{2+} influx is mediated by two VGCCs that exhibit two different kinetics of activation and that are presumably associated with two distinct molecular pathways. In particular, P/Q-type VGCCs are believed to trigger endocannabinoid release and short-term synaptic depression (Rancz and Häusser, 2006). The scheme of activation of the two distinct sets of functionally-coupled channels is illustrated in Fig. 10.

A potential role of A-type VGKCs in synaptic plasticity

The scheme of Fig.10 also shows the result of blocking or inactivating A-type VGKCs. As these channels prevent the activation of the second set of channels when the dendrite is hyperpolarised, the modulation of this channel by synaptic transmission may provide a mechanism for triggering a CF non-linear behaviour playing a role in associative plasticity. Indeed, it has been shown that A-type VGKCs are modulated by type-1 metabotropic glutamate receptors (Otsu et al., 2014) and this mechanism can play a role when the CF-EPSP is concomitant with PF activation. A-type VGKCs can also be rapidly inactivated by depolarisation produced by excitatory postsynaptic potentials, driving the dendrite to a depolarised state. This mechanism occurs in the dendrites of CA1 hippocampal pyramidal neurons where inactivation of A-type VGKCs by Schaffer collateral EPSPs leads to boosting of backpropagating action potentials, a mechanism playing a role in hebbian plasticity at these synapses (Magee and Johnston, 1997). While A-type VGKCs can act as functional trigger of synaptic plasticity, these channels can be potentially the target of meta-plasticity mechanisms to regulate dendritic functions, in particular with respect to membrane excitability. In CA1 hippocampal pyramidal neurons, coupling between local dendritic spikes and the soma can be modified in a branch-specific manner through regulation of dendritic A-type K^+ channels, a phenomenon that allows spatio-temporal correlation of synaptic inputs (Losonczy et al., 2008). In the cerebellum, this phenomenon occurs in the case of long-term potentiation of mossy fibre inputs to granule cells (Rizwan et al., 2016).

Relevance of our approach in the understanding of synergistic behaviours of ion channels

Voltage-gated and Ca^{2+}-activated ion channels shape the integration of incoming inputs in dendritic compartments and determine the pattern of V_m and Ca^{2+} influx (Magee and Johnston, 2005). In particular, each ion channel contributes to the V_m transient that in turn regulates the state of the channel (open, close or inactivated). This patterning of mutual interactions determines a global synergy with sets of distinct channels that are functionally coupled. Hence, the understanding of dendritic integration relies on the precise reconstruction of the kinetics of all principal channels underlying the response of a dendritic compartment to a given physiological input. This concept also applies to dendritic abnormal behaviours associated with channelopathies, such as the reported cases in Fragile X syndrome (Zhang et al., 2014; Brager and Johnston, 2014). Yet, the direct measurement of diverse ionic currents, mediated by different ions, is beyond available experimental techniques. In the last few years, we developed techniques to directly measure the kinetics of Ca^{2+} currents mediated by VGCCs in the dendrites of CA1 hippocampal pyramidal neurons (Jaafari et al., 2014; Jaafari et al., 2015; Jaafari and Canepari, 2016) and of PNs (Ait Ouares et al., 2016), starting from high-temporal resolution Ca^{2+} imaging. In the present work we used an alternative strategy to extract, indirectly, all the Ca^{2+} and K^+ currents underlying the CF-mediated signals, using the NEURON simulation environment (Hines and Carnevale, 1997) applied to the same type of recordings, combined with V_m imaging. This novel approach allowed us reconstructing the functional interaction among individual channels demonstrating the role of A-type VGKCs in controlling the activation of P/Q-type VGCCs. Thus, it was possible for the first time to deduce the kinetics of several Ca^{2+} and K^+ channels in parallel. It should be highlighted that a

492 single compartment model, or a multi-compartment model with a few compartments, are not a realistic
493 neuronal model of a PN since they don't account neither for the precise morphology of the cell nor for the
494 mechanisms present in small protrusions like dendritic spines. Yet, our approach is based on the
495 concept that fewer parameters allow better constraining their values when fitting with a set of
496 experimental observations. A complex multi-compartmental model based on thousands of compartments
497 (De Schutter, 1998) can be used to predict general cell integrative behaviours leading to firing activity,
498 but is not ideal for deducing the precise kinetics of dendritic channels from detailed experimental
499 observations. Modeling a PN dendrite as a single compartment is practical because PN dendritic trees
500 comprise only two VGCCs and no voltage-gated Na^+ channels. It will be very interesting, however, to
501 implement these optimised channel models into realistic PN models to predict the major physiological
502 functions of these neurons. A single compartment approach would not be appropriate in dendrites of
503 cortical and hippocampal pyramidal neurons, because these dendrites are endowed with a more
504 complex composition of voltage gated channels and notably stronger action potential backpropagation.
505 Precisely reconstructing dendritic or axonal compartments in other systems is possible, in principle,
506 using the same approach by expanding the pharmacological analysis to all the channels involved in a
507 signal. For this purpose, the database ModelDB for NEURON simulations already includes over 1100
508 published models covering more than 130 research topics (McDougal et al., 2017) that can be used as a
509 starting framework to produce more simplified models with realistic channel kinetics matching the
510 complexity of V_m and Ca^{2+} imaging experiments at high temporal resolution. The application of this novel
511 approach also concerns the study of alterations induced by mutated proteins associated with
512 channelopathies.
513

References

Ait Ouares K, Jaafari N, Canepari M (2016) A generalised method to estimate the kinetics of fast Ca(2+) currents from Ca(2+) imaging experiments. J Neurosci. Methods 268:66 -77.

Anwar H, Hepburn I, Nedelescu H, Chen W, De Schutter E (2013) Stochastic calcium mechanisms cause dendritic calcium spike variability. J Neurosci. 2013 Oct 2;33(40):15848-67.

Anwar H, Hong S, De Schutter E (2012) Controlling Ca2+-activated K+ channels with models of Ca2+ buffering in Purkinje cells. Cerebellum 11:681-693.

Anwar H, Roome CJ, Nedelescu H, Chen W, Kuhn B, De Schutter E (2014) Dendritic diameters affect the spatial variability of intracellular calcium dynamics in computer models. Front Cell Neurosci 8:168.

Brager DH, Johnston D (2014) Channelopathies and dendritic dysfunction in fragile X syndrome. Brain Res Bull 103:11-17.

Brenowitz SD, Regehr WG (2005) Associative short-term synaptic plasticity mediated by endocannabinoids. Neuron 45:419-31.

Canepari M, Mammano F (1999) Imaging neuronal calcium fluorescence at high spatio-temporal resolution. J Neurosci. Methods 87:1 -11.

Canepari M, Vogt, KE (2008) Dendritic Spike Saturation of Endogenous Calcium Buffer and Induction of Postsynaptic Cerebellar LTP. PLoS ONE 3:e4011.

Canepari M, Vogt K, Zecevic D (2008) Combining voltage and calcium imaging from neuronal dendrites. Cell Mol Neurobiol 58:1079-1093.

Canepari M, Willadt S, Zecevic D, Vogt KE (2010) Imaging Inhibitory Synaptic Potentials Using Voltage Sensitive Dyes. Biophys J 98:2032-2040.

De Schutter E (1998) Dendritic voltage and calcium-gated channels amplify the variability of postsynaptic responses in a Purkinje cell model. J Neurophysiol 80:504-519.

De Schutter E, Bower JM (1994) An active membrane model of the cerebellar Purkinje cell II. Simulation of synaptic responses. J Neurophysiol 71:401-419.

Destexhe A, Babloyantz A, Sejnowski TJ (1993) Ionic mechanisms for intrinsic slow oscillations in thalamic relay neurons. Biophys J 65:1538-1552.

Edgerton JR, Reinhart PH (2003) Distinct contributions of small and large conductance Ca2+-activated K+ channels to rat Purkinje neuron function. J Physiol 548:53-69.

Goldman-Wohl DS, Chan E, Baird D, Heintz N (1994) Kv3.3b: a novel Shaw type potassium channel expressed in terminally differentiated cerebellar Purkinje cells and deep cerebellar nuclei. J Neurosci 14:511-522.

Hines ML, Carnevale NT (1997) The NEURON simulation environment. Neural Comput 9:1179-1209.

Hosy E, Piochon C, Teuling E, Rinaldo L, Hansel C (2011) SK2 channel expression and function in cerebellar Purkinje cells. J Physiol 589:3433-3440.

Jaafari N, Canepari M (2016) Functional coupling of diverse voltage-gated Ca(2+) channels underlies high fidelity of fast dendritic Ca(2+) signals during burst firing. J Physiol 594:967-983.

552 Jaafari N, De Waard M, Canepari M (2014) Imaging Fast Calcium Currents beyond the Limitations of
553 Electrode Techniques. Biophys J 107:1280-1288.
554 Jaafari N, Marret E, Canepari M (2015) Using simultaneous voltage and calcium imaging to study fast
555 Ca2+ channels. Neurophotonics 2:021010.
556 Llano I, Marty A, Armstrong CM, Konnerth A (1991) Synaptic- and agonist-induced excitatory currents of
557 Purkinje cells in rat cerebellar slices. J Physiol 434:183-213.
558 Lee SH, Schwaller B, Neher E (2000) Kinetics of Ca2+ binding to parvalbumin in bovine chromaffin cells:
559 implications for [Ca2+] transients of neuronal dendrites. J Physiol 525:419-432.
560 Losonczy A, Makara JK, Magee JC (2008) Compartmentalized dendritic plasticity and input feature
561 storage in neurons. Nature 452:436-441.
562 Magee JC, Johnston D (1997) A synaptically controlled, associative signal for Hebbian plasticity in
563 hippocampal neurons. Science 275:209-213.
564 Magee JC, Johnston D. Plasticity of dendritic function. Curr Opin Neurobiol 15:334-342.
565 Marcaggi P, Attwell D (2005) Endocannabinoid signaling depends on the spatial pattern of synapse
566 activation. Nat Neurosci 8:776-781.
567 McDougal RA, Morse TM, Carnevale T, Marenco L, Wang R, Migliore M, Miller PL, Shepherd
568 GM, Hines ML (2017) Twenty years of ModelDB and beyond: building essential modeling tools for
569 the future of neuroscience. J Comput Neurosci 42:1-10.
570 Nägerl UV, Novo D, Mody I, Vergara JL (2000) Binding kinetics of calbindin-D(28k) determined by flash
571 photolysis of caged Ca(2+) Biophys J 79:3009-3018.
572 Otsu Y, Marcaggi P, Feltz A, Isope P, Kollo M, Nusser Z, Mathieu B, Kano M, Tsujita M, Sakimura K,
573 Dieudonné S (2014) Activity-dependent gating of calcium spikes by A-type K+ channels controls
574 climbing fiber signaling in Purkinje cell dendrites. Neuron 84:137-151.
575 Rancz EA, Häusser M (2006) Dendritic calcium spikes are tunable triggers of cannabinoid release and
576 short-term synaptic plasticity in cerebellar Purkinje neurons. J Neurosci 26:5428-5437.
577 Safo PK, Regehr WG (2005) Endocannabinoids control the induction of cerebellar LTD. Neuron 48:647-
578 659.
579 Schmidt H, Stiefel KM, Racay P, Schwaller B, Eilers J (2003) Mutational analysis of dendritic Ca2+
580 kinetics in rodent Purkinje cells: role of parvalbumin and calbindin D28k. J Physiol 551:13-32.
581 Silver RA, Momiyama A, Cull-Candy SG (1998) Locus of frequency-dependent depression identified with
582 multiple-probability fluctuation analysis at rat climbing fibre-Purkinje cell synapses. J Physiol
583 510:881-902.
584 Solinas S, Forti L, Cesana E, Mapelli J, De Schutter E, D'Angelo E (2007) Computational reconstruction
585 of pacemaking and intrinsic electroresponsiveness in cerebellar Golgi cells. Front Cell Neurosci 1:2.
586 Stocker M (2004) Ca(2+)-activated K+ channels: molecular determinants and function of the SK family.
587 Nat Rev Neurosci 5:758-770.
588 Usowicz MM, Sugimori M, Cherksey B, Llinás R (1992) P-type calcium channels in the somata and
589 dendrites of adult cerebellar Purkinje cells. Neuron 9:1185-1199.

590 Veys K, Snyders D, De Schutter E (2013) Kv3.3b expression defines the shape of the complex spike in
591 the Purkinje cell. Front Cell Neurosci 7:205.
592 Vogt KE, Canepari M (2010) On the induction of postsynaptic granule cell-Purkinje neuron LTP and LTD.
593 Cerebellum 9:284-290.
594 Vogt KE, Gerharz S, Graham J, Canepari M (2011a) High-resolution simultaneous voltage and Ca^{2+}
595 imaging. J Physiol 589:489-494.
596 Vogt KE, Gerharz S, Graham J, Canepari M (2011b) Combining membrane potential imaging with L-
597 glutamate or GABA photorelease. PLoS ONE 6:e24911.
598 Zagha E, Manita S, Ross WN, Rudy B (2010) Dendritic Kv3.3 potassium channels in cerebellar purkinje
599 cells regulate generation and spatial dynamics of dendritic Ca2+ spikes. J Neurophysiol 103:3516-
600 3525.
601 Zhang Y, Bonnan A, Bony G, Ferezou I, Pietropaolo S, Ginger M, Sans N, Rossier J, Oostra B,
602 LeMasson G, Frick A (2014) Dendritic channelopathies contribute to neocortical and sensory
603 hyperexcitability in Fmr1(-/y) mice. Nat Neurosci 17:1701-1709.
604 Zoukimian C, Meudal H, De Waard S, Ait Ouares K, Nicolas S, Canepari M, Béroud R, Landon C, De
605 Waard M, Boturyn D (2018) Synthesis by native chemical ligation and characterization of the
606 scorpion toxin AmmTx3. Bioorg Med Chem, *in press* (doi: 10.1016/j.bmc.2018.12.009).
607

608 **Figure Legend**

609

610 **Figure 1.** V_m calibration protocol and illustration of NEURON model. ***A,*** On the left, fluorescence
611 reconstruction of a PN with three regions of interest (*R1*, *R2* and *R3*). From the resting V_m (-67 mV),
612 negative or positive current pulses of 1 s duration were delivered from the recording electrode. On the
613 right, somatic V_m and the VSD-$\Delta F/F_0$ signals in *R1-R3* associated with the current pulses. The VSD-
614 $\Delta F/F_0$ signal in each regions is converted into mV to quantify the V_m transient associated with the CF-
615 EPSP assuming that the resting V_m is uniform (*int* state) and that the hyperpolarising pulse spreads into
616 the dendrites without attenuation (*hyp* state). The protocol also allows determining the dendritic V_m
617 associated with the strongest depolarising pulse (*dep* state). ***B,*** A dendritic region of ~17X17 μm^2 is
618 approximated with a cylinder of 4 µm diameter and 20 µm length in the NEURON model. The model
619 contains P/Q type and T-type Ca^{2+} channels; SK, BK, A-type K^+ channels and a generic HVAK. It
620 includes four buffers: a fast immobile buffer, the Ca^{2+} indicator (either Fura-FF or OG5N), Parvalbumin
621 and Calbindin D-28k. It also includes Ca^{2+} extrusion and a LEAK channel.

622

623 **Figure 2.** Combined V_m and Ca^{2+} transients associated with the CF-EPSP. ***A,*** On the bottom,
624 fluorescence reconstruction of a representative PN with two regions of interest indicated (*R1* and *R2*).
625 On the top, somatic V_m associated with a CF-EPSP at three different initial V_m: hyperpolarised (*hyp* blue
626 trace); intermediate (*int* green trace); depolarised (*dep* red trace). ***B,*** On the top, dendritic V_m in *R1* and
627 *R2* calibrated as illustrated in Fig. 1A corresponding to the somatic CF-EPSPs in panel *A*. On the
628 bottom, corresponding FuraFF $\Delta F/F_0$ signals. ***C,*** Analysis of the V_m and Ca^{2+} maxima (max) associated
629 with signals in *R1* reported in panel *B*; the 1st max of the V_m and Ca^{2+} transients is calculated within the
630 first 4 ms after the CF stimulation; the 2nd max of the V_m and Ca^{2+} transients is calculated between 4 and
631 14 ms after the CF stimulation; blue traces and characters are for the *hyp* state; green traces and
632 characters are for the *int* state; red traces and characters are for the *dep* state. ***D,*** Mean ± SD for 19
633 regions in 12 cells analysed as illustrated in panel *C*; The *hyp* states (blue columns) were with initial V_m
634 between -87 mV and -74 mV; The *int* states (green columns) were with initial V_m between -68 mV and -
635 61 mV; The *dep* states (red columns) were with initial V_m between -54 mV and -46 mV; the symbol "*"
636 indicates a significant increase in the max ($p < 0.005$, paired t-test).

637

638 **Figure 3.** Dendritic Ca^{2+} channels activated by the CF-EPSP. ***A,*** On the left, fluorescence reconstruction
639 of a PN with two regions of interest indicated (*R1* and *R2*); *R1* is next to a pipette delivering 1 µM of the
640 P/Q-type VGCC inhibitor AgaIVA; *R2* is >50 µm from the application pipette. On the right (top), somatic
641 V_m associated with CF-EPSPs in control conditions and after local application of AgaIVA at three
642 different initial V_m: *hyp* (blue trace); *int* (green trace); *dep* (red trace). On the right (bottom) the
643 corresponding OG5N $\Delta F/F_0$ signals. ***B,*** In another PN, same as *A*, but with the pipette delivering the T-
644 type VGCC inhibitors ML (5 µM) and NNC (30 µM). ***C,*** In another PN, same as *A*, but with the pipette
645 delivering both the P/Q VGCC inhibitor AgaIVA (1 µM) and the T-type VGCC inhibitors ML (5 µM) and

NNC (30 μM). ***D,*** In three other PNs, from a region next to a pipette delivering a VGCC blocker, the OG5N $\Delta F/F_0$ signals associated with CF-EPSPs in control conditions and after local application of 20 μM of the L-type VGCC inhibitor Isr, of 5 μM of the N-type VGCC inhibitor PD or 1 μM of the R-type VGCC inhibitor SNX at the three different initial V_m.

Figure 4. Quantitative analysis of dendritic Ca^{2+} channels activated by the CF-EPSP. On the left, from two representative cells, OG5N $\Delta F/F_0$ signals associated with CF-EPSPs in control conditions at three different initial V_m: *hyp* (blue trace); *int* (green trace); *dep* (red trace); superimposed (gray traces) are the OG5N $\Delta F/F_0$ signals after local application of either 1 μM of the P/Q-type VGCC inhibitor AgaIVA or of the T-type VGCC blockers ML (5 μM) and NNC (30 μM); the 1^{st} max of the Ca^{2+} transient is calculated within the first 4 ms after the CF stimulation; the 2^{nd} max of the Ca^{2+} transient is calculated between 4 and 14 ms after the CF stimulation; the percentages from control $\Delta F/F_0$ maxima after application of the VGCC blockers are reported above or below the arrows. On the right, mean ± SD of the percentages from control $\Delta F/F_0$ maxima after application of the VGCC inhibitors AgaIVA (N = 6 cells), ML+NNC (N = 6 cells), AgaIVA+ML+NNC (N = 6 cells), Isr (N = 4 cells), PD (N = 4 cells) or SNX (N = 4 cells); gray columns are the statistics of the 1^{st} max; white columns are the statistics of the 2^{nd} max; the symbol "*" indicates a significant change in the max ($p < 0.005$, paired t-test).

Figure 5. Dendritic A-type VGKCs activated by the CF-EPSP. ***A,*** On the left, fluorescence reconstruction of a PN with a region of interest indicated next to a pipette delivering 1 μM of the A-type VGKC inhibitor AmmTx3. On the right (top), somatic V_m associated with CF-EPSPs in control conditions and after local application of AmmTx3 at three different initial V_m: *hyp* (blue trace); *int* (green trace); *dep* (red trace). On the right (bottom) the corresponding OG5N $\Delta F/F_0$ signals. ***B,*** On the left , from the cell in *A*, OG5N $\Delta F/F_0$ signals associated with CF-EPSPs in control conditions at the three different initial V_m; superimposed (gray traces) are the OG5N $\Delta F/F_0$ signals after local application of either 1 μM AmmTx3; the 1^{st} max of the Ca^{2+} transient is calculated within the first 4 ms after the CF stimulation; the percentages from control $\Delta F/F_0$ maxima after application of the VGCC blockers are reported above the arrows. On the right, mean ± SD of the percentages from control $\Delta F/F_0$ maxima after application of AmmTx3 (N = 6 cells); gray columns are the statistics of the 1^{st} max; white columns are the statistics of the 2^{nd} max; the symbol "*" indicates a significant change in the max ($p < 0.005$, paired t-test).

Figure 6. Dendritic Ca^{2+}-activated K^+ channels activated by the CF-EPSP. ***A,*** On the left, fluorescence reconstruction of a PN with a region of interest indicated next to a pipette delivering 1 μM of the BK channel inhibitor iberiotoxin. On the right (top), somatic V_m associated with CF-EPSPs in control conditions and after local application of iberiotoxin at three different initial V_m: *hyp* (blue trace); *int* (green trace); *dep* (red trace). On the right (bottom) the corresponding OG5N $\Delta F/F_0$ signals. ***B,*** In another PN, same as *A* but with the pipette delivering 1 μM of the SK channel inhibitor apamin. ***C,*** Mean ± SD of the percentages from control $\Delta F/F_0$ maxima after application of iberiotoxin (N = 5 cells) or apamin (N = 6

cells); gray columns are the statistics of the 1st max; white columns are the statistics of the 2nd max. ***C,*** On the left, from the cell in *A*, OG5N $\Delta F/F_0$ signal associated with the CF-EPSP at *dep* state in control condition and after addition of iberiotoxin (gray trace). On the right, from the cell in *B*, OG5N $\Delta F/F_0$ signal associated with the CF-EPSP at *hyp* state in control condition and after addition of apamin (gray trace).

Figure 7. NEURON model of 4 PN dendritic compartments reproducing V_m and Ca^{2+} transients associated with the CF-EPSP. On the left, experimental dendritic V_m and Ca^{2+} transients associated with CF-EPSPs from 4 selected cells at three different initial V_m: hyperpolarised (*hyp*, blue trace); intermediate (*int*, green trace); depolarised (*dep*, red trace). On the right, simulations of dendritic V_m and Ca^{2+} transients associated with CF-EPSPs reproducing experimental data (gray traces).

Figure 8. Simulations of block of P/Q-type VGCCs, T-type VGCCs, A-type VGKCs, BK and SK Ca^{2+} activated K^+ channels from a NEURON model. Simulated Ca^{2+} transients (OG5N) associated with CF-EPSPs at three different initial V_m in control condition and after reduction of 90% of one individual channels from Cell 1 model variant reported in Fig. 7. For each case of 90% channel reduction, traces under control conditions are reported in gray.

Figure 9. Individual currents extracted from NEURON model. Ca^{2+} currents of P/Q and T channels and K^+ currents of A, BK, SK and HVAK channels from the simulations of Cell 1 model variant reported in Fig. 7. Simulations were at hyp (blue traces), int (green traces) and dep (red traces) states in control conditions, and at hyp (purple traces) after blocking 90% of A-type VGKCs, superimposed to currents in control conditions (gray traces).

Figure 10. Channel activation following CF-EPSPs at hyperpolarised and depolarised states. ***A***, In control conditions, at *hyp* state, the CF-EPSP activates T-type channels, that activate SK channels, and A channels that limit activation P/Q and HVAK channels; at *dep* state, state, the CF-EPSP activates P/Q-type channels, that activate BK channels, and HVAK channels, while T channels and A channels are inactivated. ***B***, When A channels are blocked or inactivated, at hyp state the CF-EPSP also activates P/Q-type channels, that activate BK channels, and HVAK channels.

Table 1

Signal (% control) / Channel block		*Hyp*		*Int*		*Dep*	
		1st max	2nd max	1st max	2nd max	1st max	2nd max
P/Q	+1 μM AgaIVA (N = 6 cells)	50 ± 24*	90 ± 30	25 ± 12*	61 ± 31	10 ± 5*	6 ± 4
	***-90% P/Q channels* (N = 4 simulations)**	***74 ± 2***	***92 ± 3***	***13 ± 2***	***22 ± 6***	***6 ± 2***	***4 ± 1***
T	+5 μM ML+30 μM NNC (N = 6 cells)	52 ± 24*	21 ± 9*	94 ± 8	45 ± 15*	100 ± 4	99 ± 11
	***-90% T channels* (N = 4 simulations)**	***19 ± 3***	***12 ± 2***	***89 ± 3***	***90 ± 3***	***100***	***100***
A	+1 μM AmmTx3 (N = 6 cells)	151 ± 34*	187 ± 44*	114 ± 8*	160 ± 33*	102 ± 4	102 ± 5
	***-90% A channels* (N = 4 simulations)**	***247 ± 39***	***281 ± 34***	***104 ± 2***	***180 ± 68***	***100***	***100***
BK	+1 μM iberiotoxin (N = 5 cells)	97 ± 5	99 ± 5	98 ± 3	98 ± 4	98 ± 9	106 ± 5
	***-90% BK channels* (N = 4 simulations)**	***100 ± 1***	***101 ± 1***	***100 ± 1***	***100 ± 1***	***101 ± 1***	***117 ± 18***
SK	+1 μM apamin (N = 6 cells)	101 ± 9	101 ± 10	100 ± 8	99 ± 6	103 ± 7	97 ± 8
	***-90% SK channels* (N = 4 simulations)**	***100 ± 1***	***101 ± 1***	***100 ± 1***	***100 ± 1***	***100 ± 1***	***103 ± 5***

Table 1. Comparison of the percentage of the control Ca^{2+} transient (mean ± SD of the 1st and 2nd maxima) produced by the pharmacological block of a channel type, in the case of experimental data, with the percentage of the control Ca^{2+} transient produced by the elimination of 90% of the channel in the case of simulations. The number of cells and the number of simulations used for the statistics is indicated. Simulations were performed by using 2 mM OG5N in the four variants of the model reported in Fig. 7.

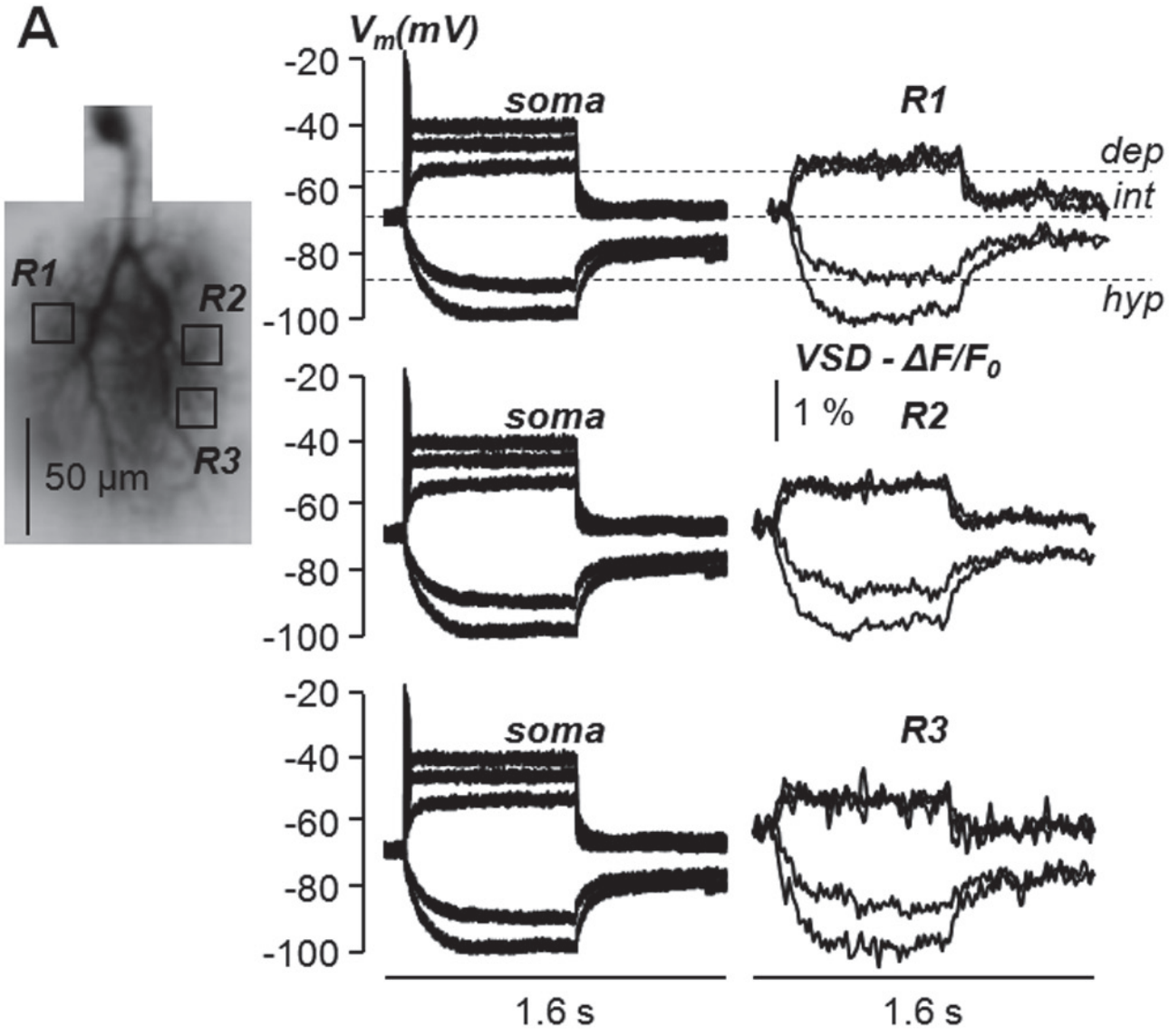

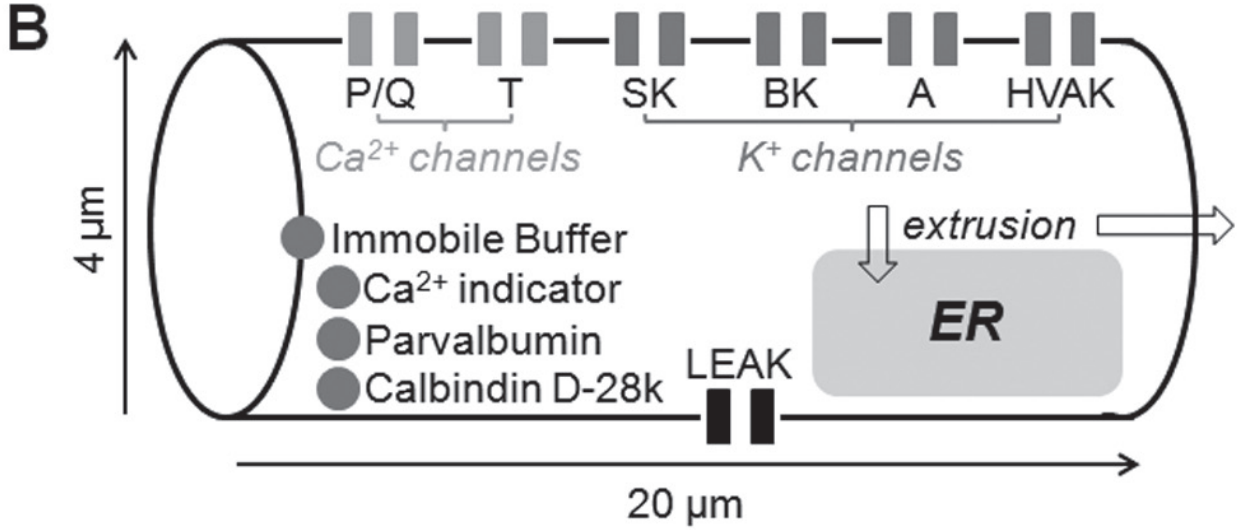

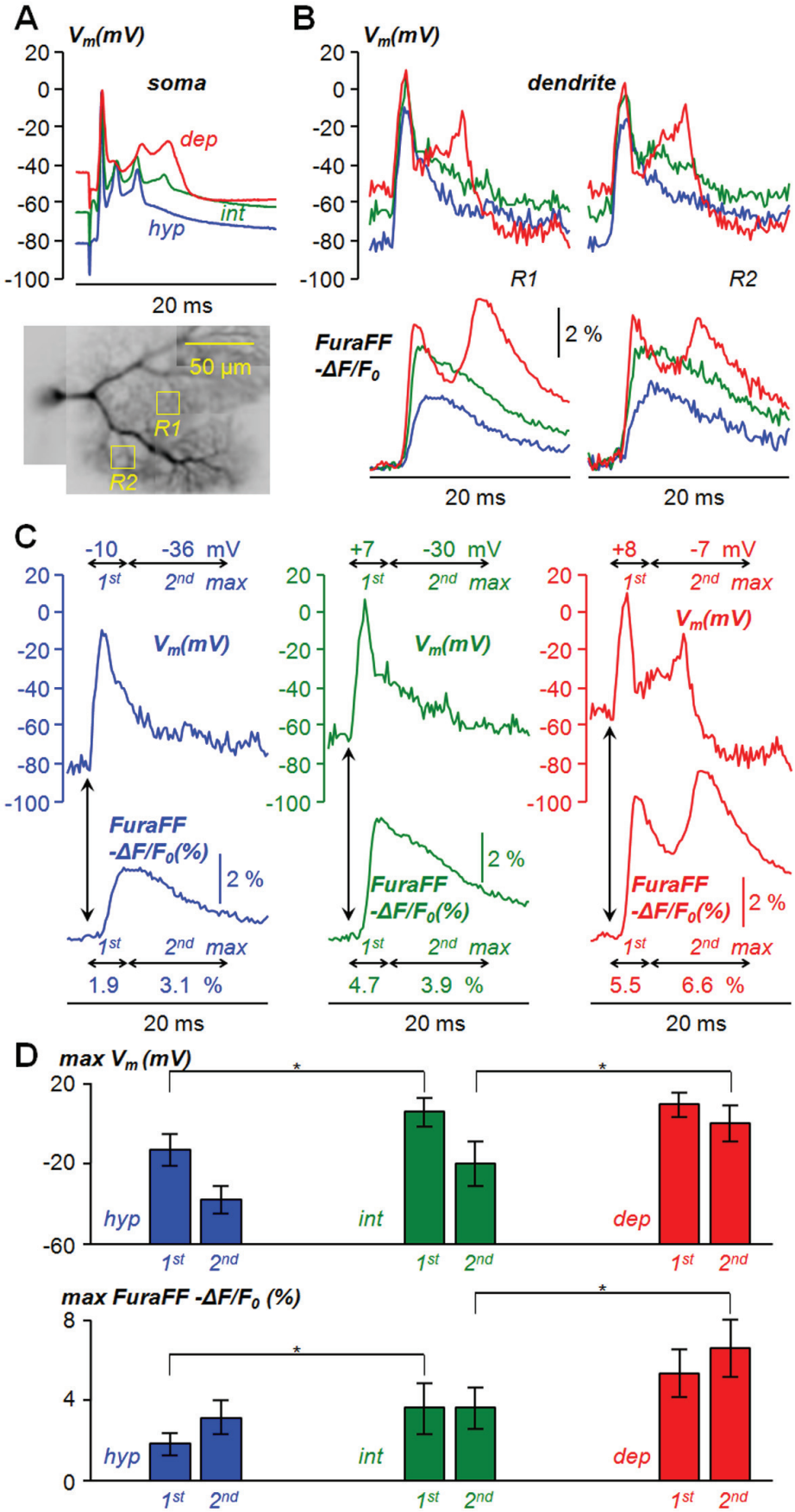

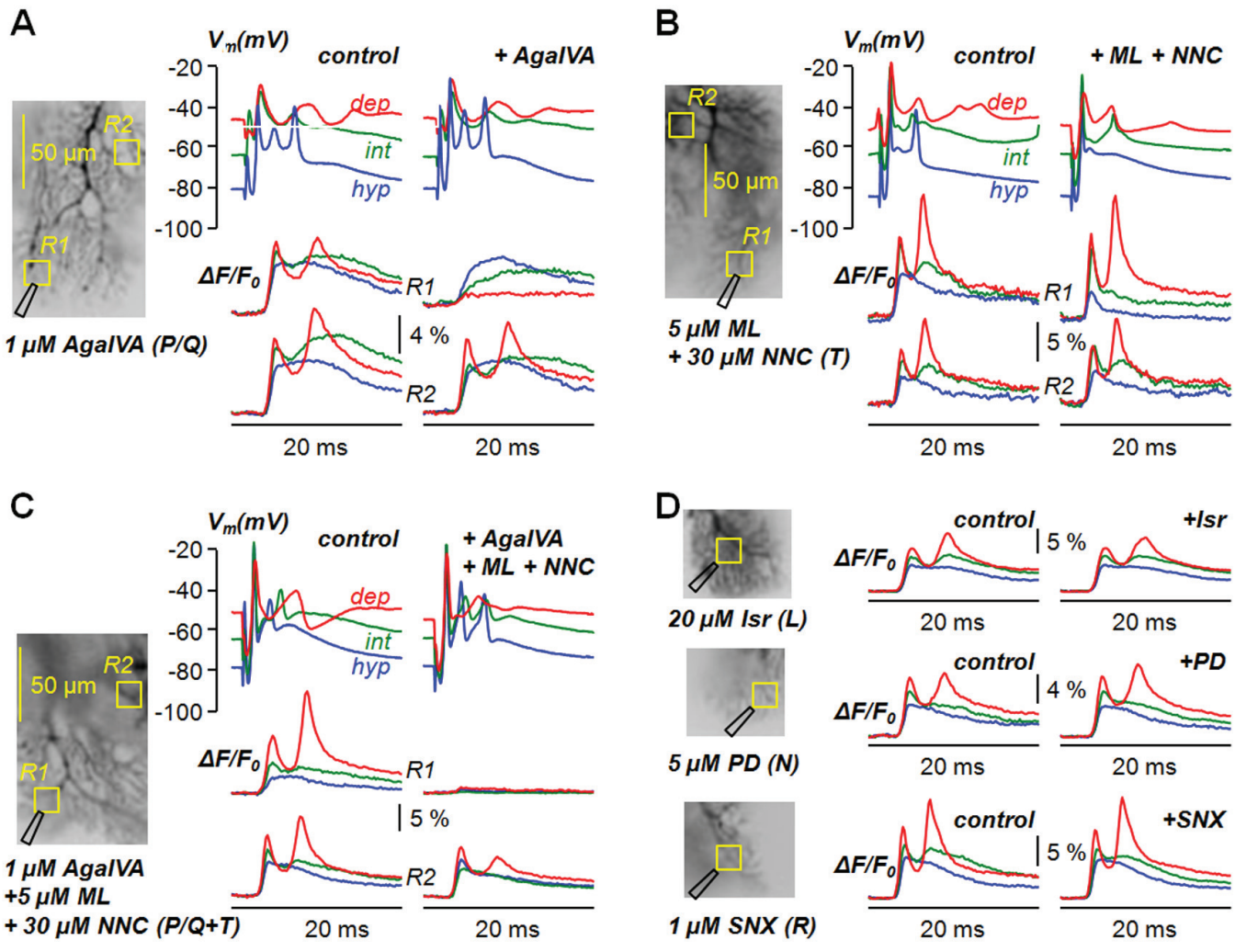

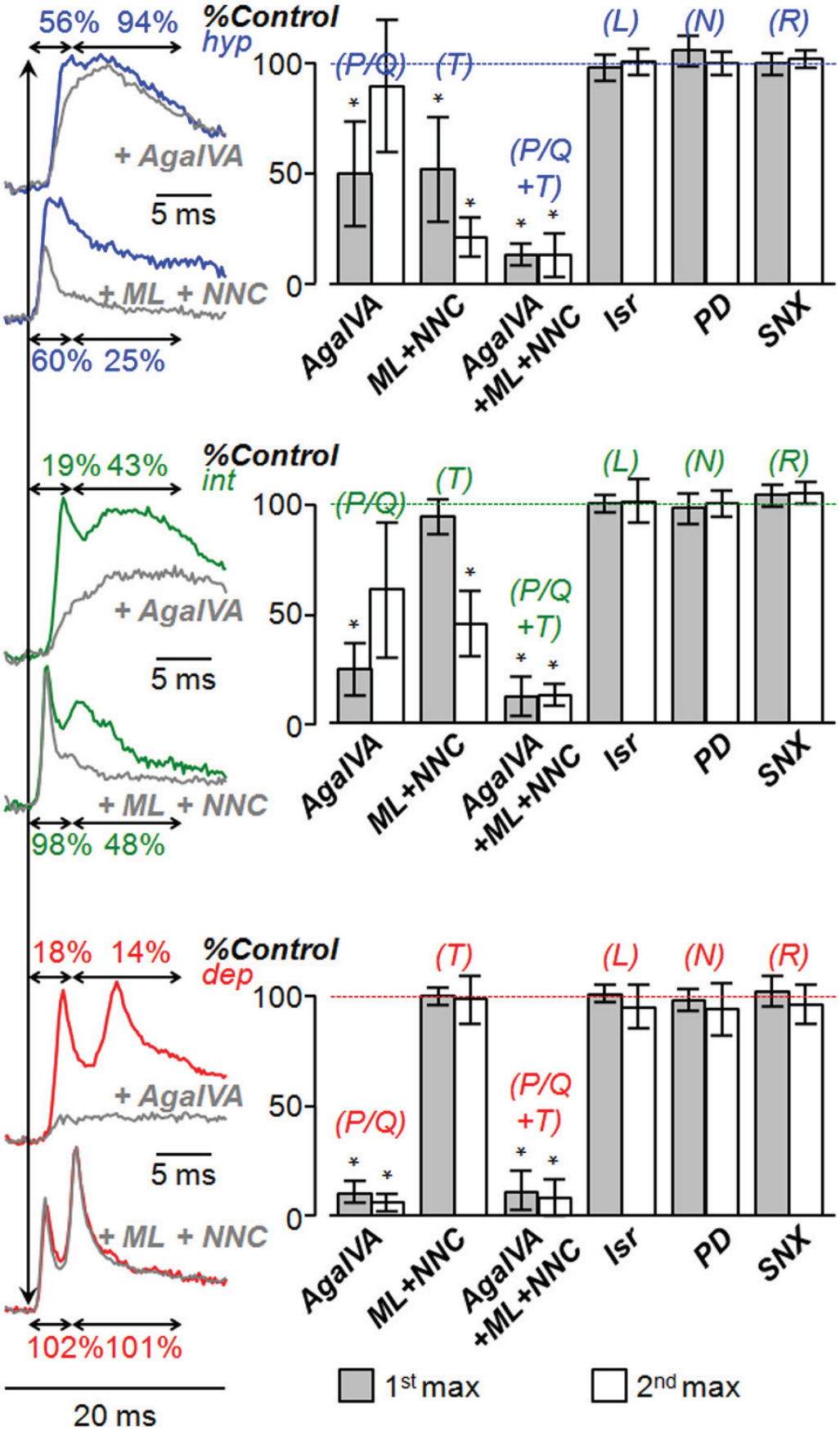

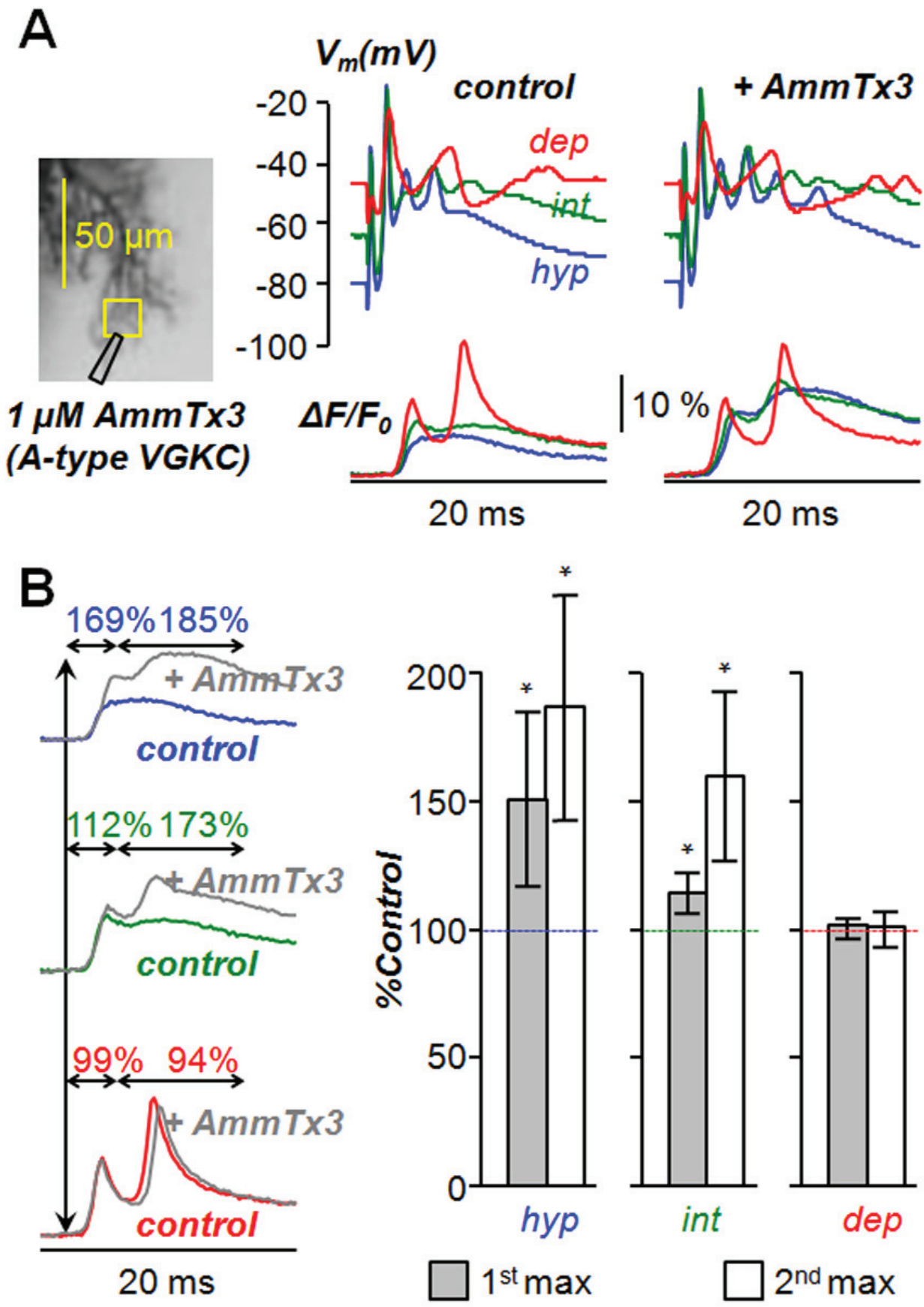

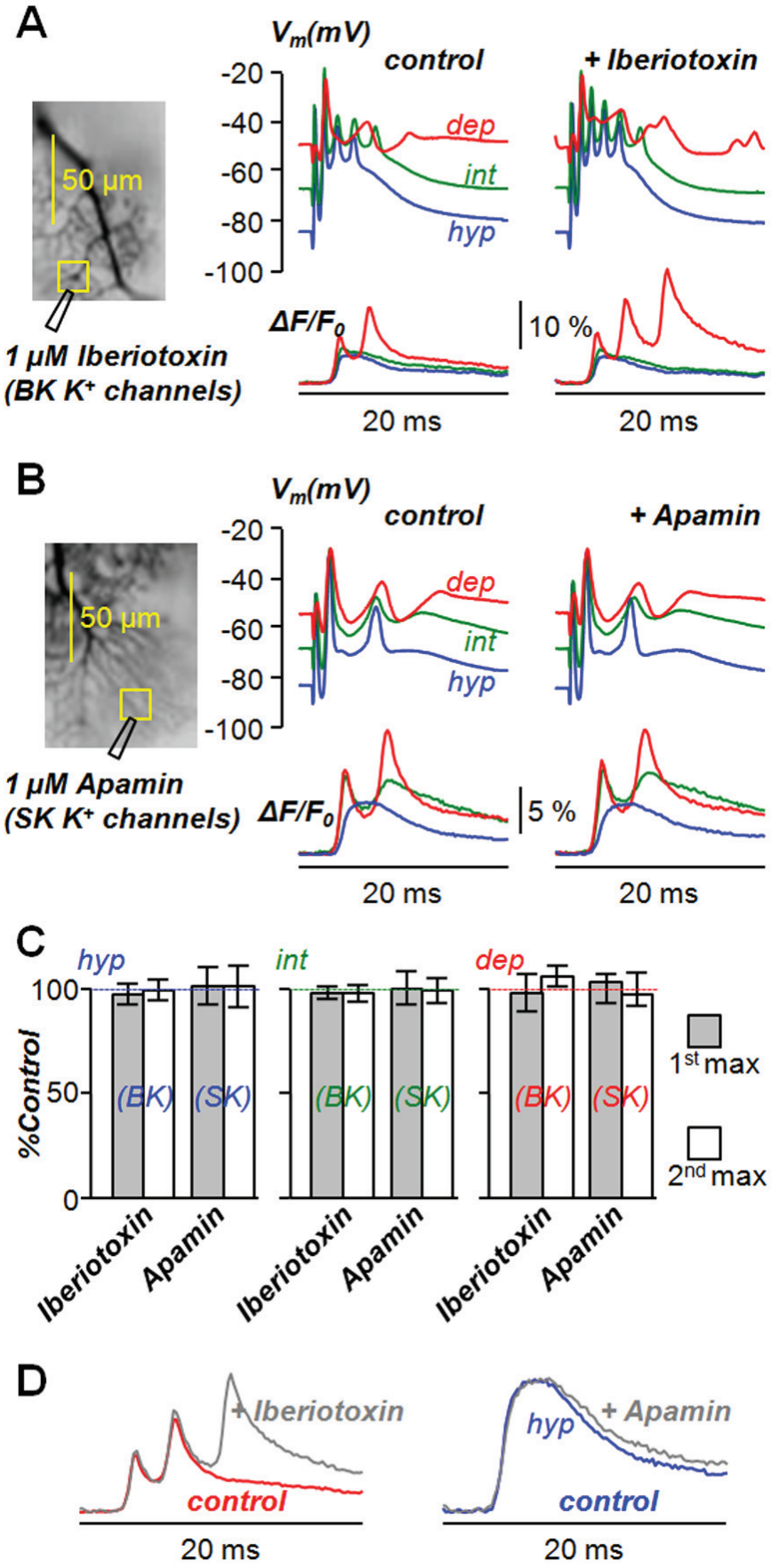

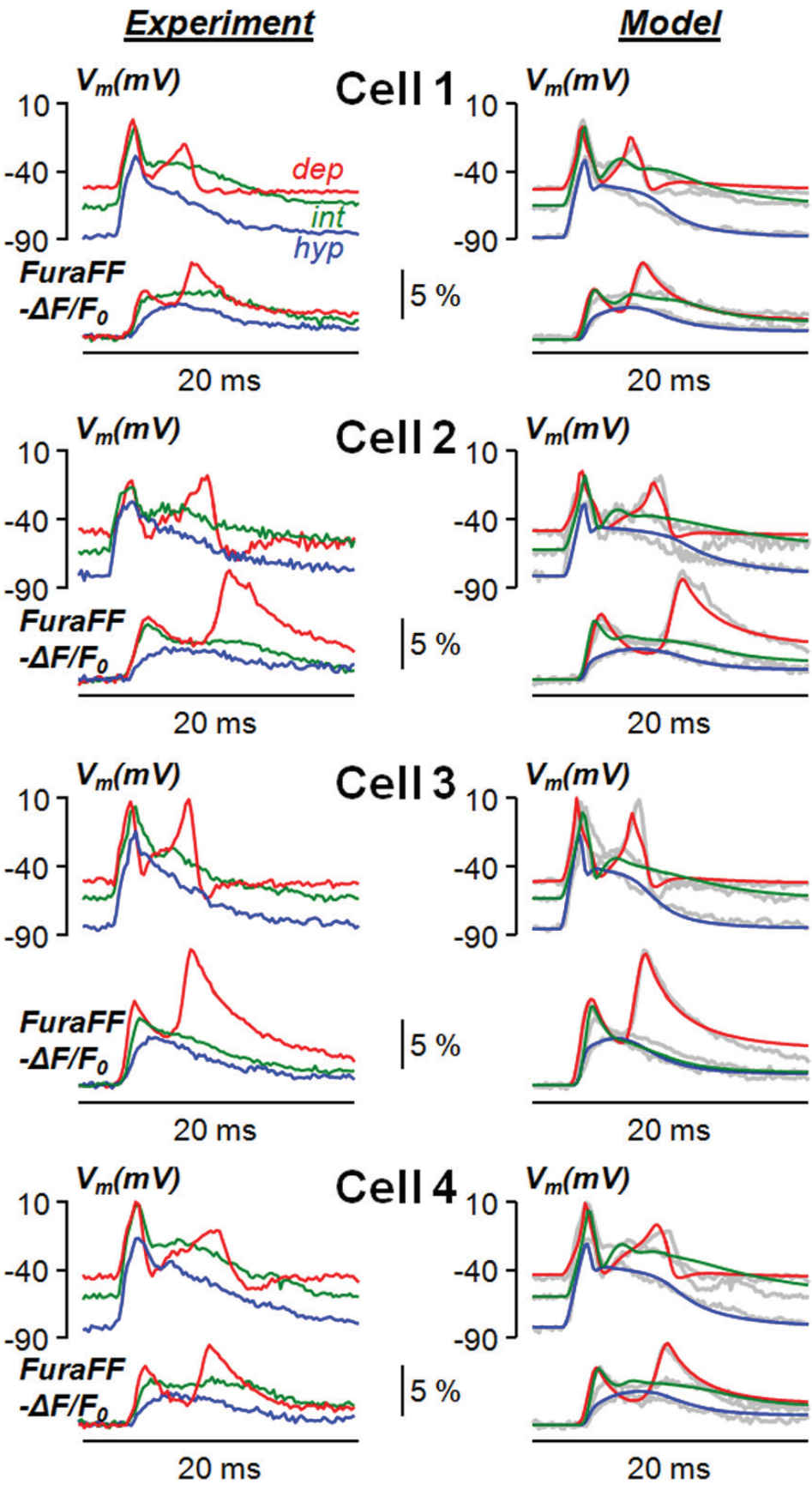

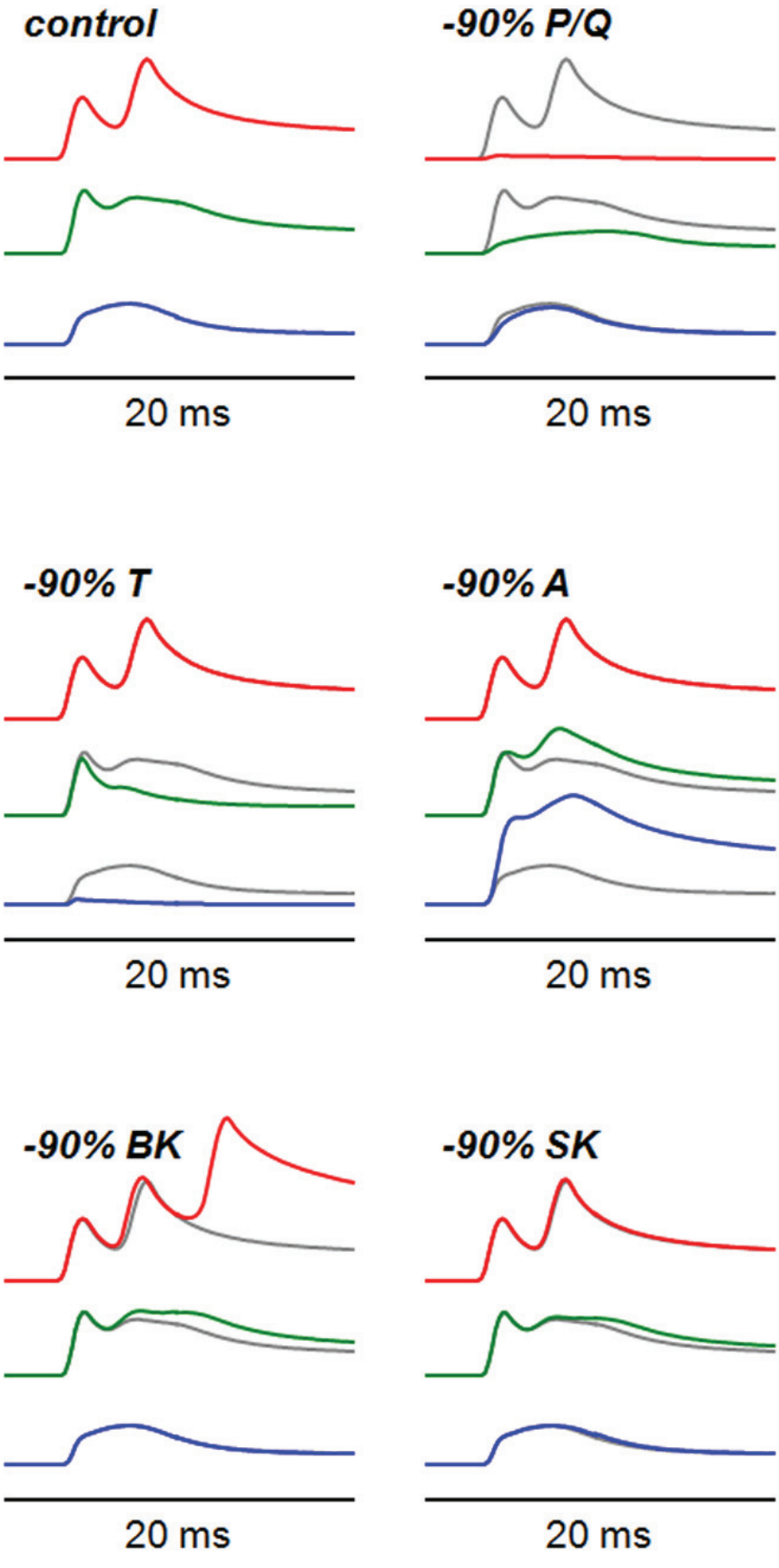

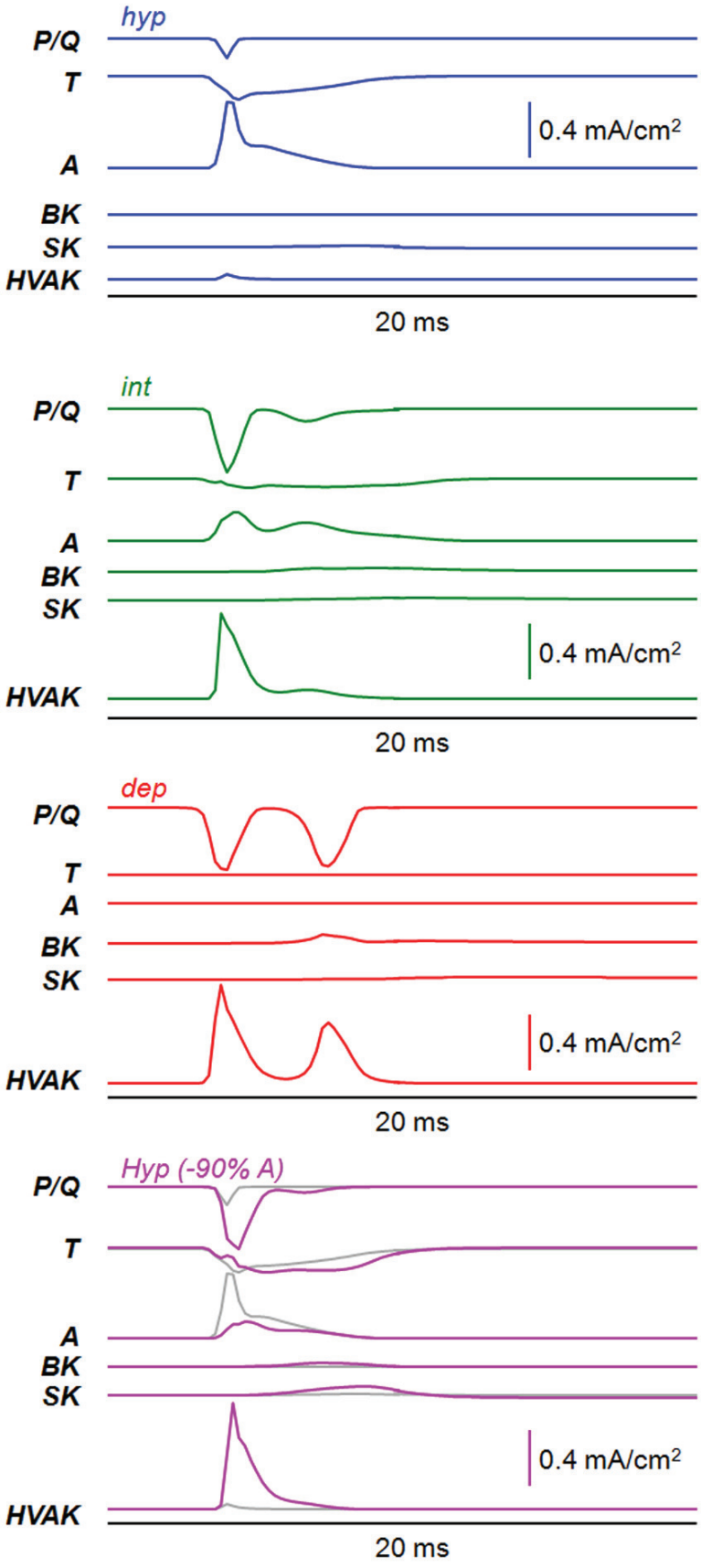

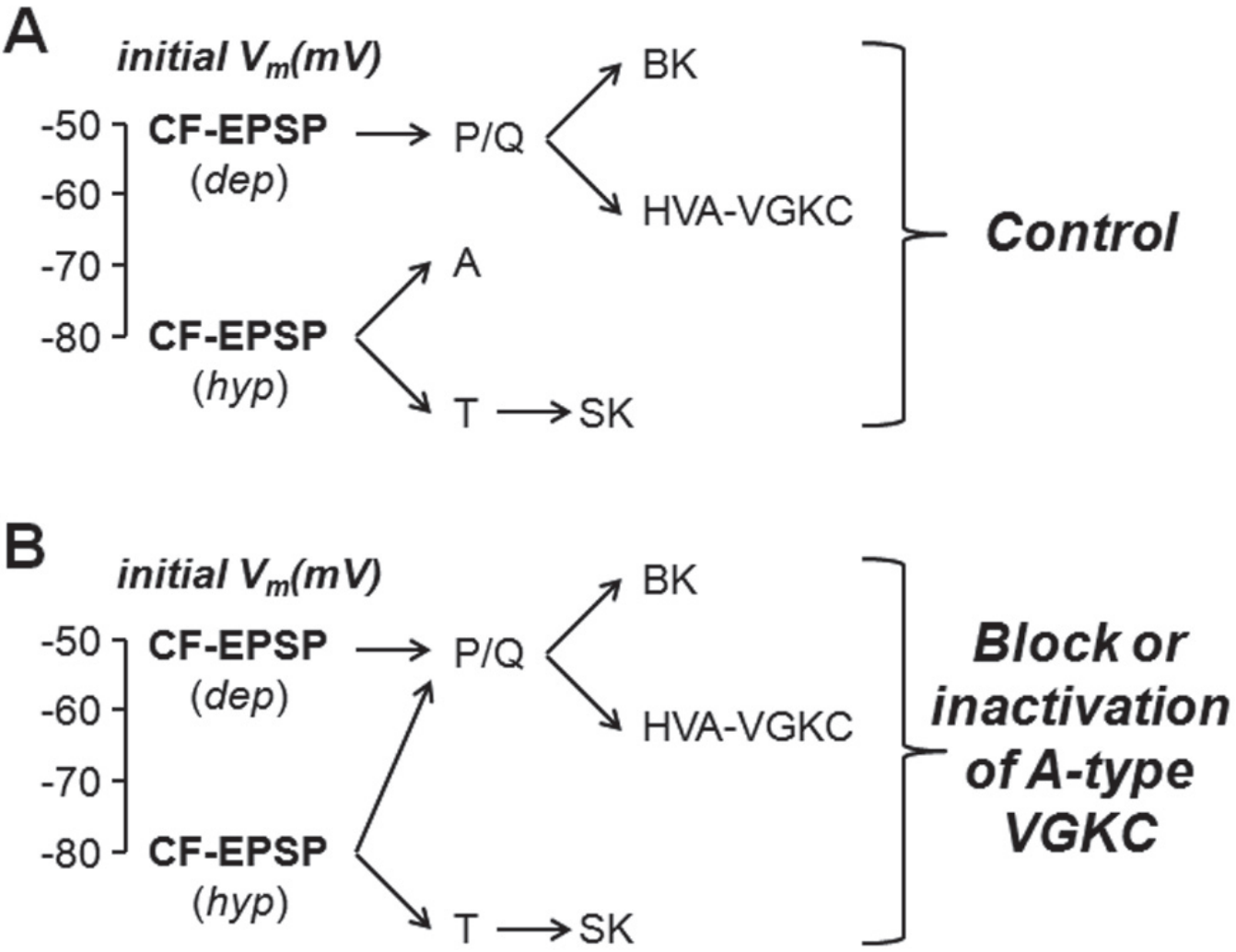

Table 1

Signal (% control) / Channel block		*Hyp*		*Int*		*Dep*	
		1st max	2nd max	1st max	2nd max	1st max	2nd max
P/Q	+1 μM AgaIVA (N = 6 cells)	50 ± 24*	90 ± 30	25 ± 12*	61 ± 31	10 ± 5*	6 ± 4
	***-90% P/Q channels* (N = 4 simulations)**	***74 ± 2***	***92 ± 3***	***13 ± 2***	***22 ± 6***	***6 ± 2***	***4 ± 1***
T	+5 μM ML+30 μM NNC (N = 6 cells)	52 ± 24*	21 ± 9*	94 ± 8	45 ± 15*	100 ± 4	99 ± 11
	***-90% T channels* (N = 4 simulations)**	***19 ± 3***	***12 ± 2***	***89 ± 3***	***90 ± 3***	***100***	***100***
A	+1 μM AmmTx3 (N = 6 cells)	151 ± 34*	187 ± 44*	114 ± 8*	160 ± 33*	102 ± 4	102 ± 5
	***-90% A channels* (N = 4 simulations)**	***247 ± 39***	***281 ± 34***	***104 ± 2***	***180 ± 68***	***100***	***100***
BK	+1 μM iberiotoxin (N = 5 cells)	97 ± 5	99 ± 5	98 ± 3	98 ± 4	98 ± 9	106 ± 5
	***-90% BK channels* (N = 4 simulations)**	***100 ± 1***	***101 ± 1***	***100 ± 1***	***100 ± 1***	***101 ± 1***	***117 ± 18***
SK	+1 μM apamin (N = 6 cells)	101 ± 9	101 ± 10	100 ± 8	99 ± 6	103 ± 7	97 ± 8
	***-90% SK channels* (N = 4 simulations)**	***100 ± 1***	***101 ± 1***	***100 ± 1***	***100 ± 1***	***100 ± 1***	***103 ± 5***

Table 1. Comparison of the percentage of the control Ca^{2+} transient (mean ± SD of the 1st and 2nd maxima) produced by the pharmacological block of a channel type, in the case of experimental data, with the percentage of the control Ca^{2+} transient produced by the elimination of 90% of the channel in the case of simulations. The number of cells and the number of simulations used for the statistics is indicated. Simulations were performed by using 2 mM OG5N in the four variants of the model reported in Fig. 7.